Supporting Information for**:**

Synthesis and Characterization of "Atlas-sphere" Copper Nanoclusters: New Insights into the Reaction of Cu^{2+} with Thiols

Andrew W. Cook[1], Zachary R. Jones[3], Guang Wu[1], Simon J. Teat[2], Susannah L. Scott[3]*, and Trevor W. Hayton[1]*

[1]*Department of Chemistry and Biochemistry, University of California, Santa Barbara, California 93106, United States*

[2]*Advanced Light Source, Lawrence Berkeley National Laboratory, Berkeley, California 94720, United States*

[3]*Department of Chemical Engineering, University of California, Santa Barbara, California 93106, United States*

*hayton@chem.ucsb.edu

*sscott@engineering.ucsb.edu

Table of Contents

Experimental Details

All reactions and subsequent manipulations were performed under anaerobic and anhydrous conditions under an atmosphere of nitrogen. Hexanes was dried using a Vacuum Atmospheres DRI-SOLV Solvent Purification system and stored over 3Å sieves for 24 h prior to use. Dichloromethane (CH_2Cl_2) and pentane were dried on an MBraun solvent purification system. Tetrahydrofuran (THF) was dried by distillation from calcium hydride (CaH_2) followed by distillation from sodium benzophenone ketyl. Dibenzyl ether and pyridine were degassed and dried over 3Å molecular sieves for 72 h prior to use. THF-d_8, C_5D_5N (py-d_5), CD_2Cl_2, hexamethyldisiloxane (HMDSO), 1-butanethiol, 2-phenylethanethiol, and 1-dodecanethiol were dried over 3Å molecular sieves for 24 h prior to use. Na(S^nBu) and $[Cu_{14}H_{12}(phen)_6(PPh_3)_4][Cl]_2$ were prepared according to the literature procedure.[1-2] All other reagents were purchased from commercial suppliers and used as received.

All NMR spectra were collected at room temperature. ^1H NMR spectra were recorded on an Agilent Technologies 400-MR DD2 400 MHz spectrometer or a Varian Unity Inova 500 MHz spectrometer. The chemical shifts of all nuclei were referenced to the residual solvent peaks. IR spectra were recorded on a Nicolet 6700 FT-IR spectrometer with a NXR FT Raman Module. Electronic absorption spectra were recorded on a UV-2401 PC Shimadzu UV-NIR spectrophotometer. The diffuse reflectance spectrum was recorded on a UV-3600 Shimadzu UV-NIR spectrophotometer equipped with an integrating sphere using a powder sample of **1**. Emission spectra were recorded on a Horiba FluoroMax 4 spectrometer equipped with a 420 nm colored glass pass filter. Electrospray ionization (ESI) mass spectra were collected in THF at the Materials Research Laboratory Shared Experimental Facilities at UCSB, using an ESI source in negative ion mode with a Waters Xevo G2-XS TOF mass spectrometer. A 0.25 mM THF solution of NEt_4Cl

was added to the mass spectra samples to enhance the ionization of the dissolved species. GC mass spectra were collected in CH_2Cl_2 at the Mass Spectrometry Facility in the Department of Chemistry and Biochemistry at UCSB on an HP 5970 mass spectrometer equipped with a J&W DB-5ms 30m GC column, with 0.25 mm ID and 0.25 μm film thickness. Mass spectra were smoothed 3 times using the mean algorithm with a smooth window of 2 channels. The XPS spectrum of a solid sample of **1** was recorded on a Kratos Axis Ultra DLD X-ray Photoelectron Spectroscopy system equipped with a monochromated Al-k alpha source (1486 eV). Survey and high-resolution scans were recorded at 160 and 20 eV pass energies, respectively. A low-energy electron flood was used for charge neutralization, and peak positions were calibrated against the aliphatic C 1s peak (285.0 eV). The thermogravimetric analysis of **1** was performed on a TA Discovery TGA. The sample was run under N_2 with a flow of 25 mL/min from 30-800 °C and a ramp rate of 10 °C/min. The sample was loaded into an alumina crucible, and then placed on a high temperature Pt pan.

X-ray Absorption Spectroscopy. The X-ray absorption spectra (XAS) were collected at the Stanford Synchrotron Radiation Lightsource (SSRL, 3-GeV ring with a current of 500mA) on beamline 7-3 with a Si(220) crystal oriented at $\phi = 90^{o}$. Samples of complexes **1** and **2** used for the XAS analysis were synthesized using dibenzyl ether as the solvent. Each spectrum was collected at 10 K under a LHe cryostat. Six individual scans were acquired, their energies aligned using the spectrum of a Cu metal calibration foil collected simultaneously, and averaged using the Athena software package. The averaged scans were subjected to linear pre-edge subtraction and normalization by edge height. Then the extended fine structure (EXAFS) function, $\chi(k)$, was isolated by subtracting a smooth, third-order polynomial approximating the absorption background of an isolated atom. The spectra were k^3-weighted and Fourier transformed prior to non-linear

curvefitting. The energy phase shift parameter (ΔE_o) was refined as a global parameter and then fixed for the remainder of the curvefitting analysis. The amplitude reduction factor, S_o^2, was fixed at 0.8 in accordance with previous analyses of Cu(I) standards and Cu-based clusters.[3-4] The scattering paths were simulated using FEFF8 and the Artemis software.[5] The number of Cu-Cu interactions were reduced to one, two, or three paths. The highest frequency paths as predicted from the FEFF calculations were selected to represent the average Cu-Cu bond lengths. The coordination number, *N*, path length, *R*, and mean-squared displacement, σ^2, were refined as variables. The values of R and σ^2 were refined first, then fixed while *N* was refined.

Attempted Synthesis of 1-Dodecanethiol-Protected Copper Nanoclusters in Dibenzyl Ether.[6] To $CuCl_2$ (93.0 mg, 0.692 mmol) in a 20 mL scintillation vial equipped with a magnetic stir bar was added dibenzyl ether (2 mL) at 25 °C to give a brown slurry. 1-dodecanethiol (0.65 mL, 2.71 mmol) was then added to this slurry via syringe. The resulting mixture was stirred for 20 min, which resulted in the dissolution of the brown solid concomitant with the deposition of a very pale, fine gray solid. The reaction mixture was then filtered through a medium porosity frit, the collected solids were rinsed with hexanes (2 × 4 mL), and the colorless filtrate was discarded. The off-white powder was then dried *in vacuo* to yield **1** (148 mg).

Attempted Synthesis of 1-Dodecanethiol-Protected Copper Nanoclusters in THF. To $CuCl_2$ (90.0 mg, 0.669 mmol) in a 20 mL scintillation vial equipped with a magnetic stir bar was added THF (2 mL) at 25 °C to give a brown slurry. 1-dodecanethiol (0.65 mL, 2.71 mmol) was added to this slurry via syringe, which resulted in the rapid dissolution of the brown solid over the course of 2 min to give a pale yellow solution. The reaction mixture was then allowed to stir for 20 min, whereupon a very pale yellow powder was deposited in the vial. The reaction mixture was then filtered through a medium porosity frit and the collected solids were rinsed with hexanes (2 × 4

mL). The resulting pale-yellow powder was then dried *in vacuo* to yield **1** (116 mg). Diffuse Reflectance UV/vis: 361 nm (sh). Fluorescence (λ_{ex} = 365 nm): 510 nm (FWHM = 130 nm). IR (KBr pellet, cm^{-1}): 716 (s), 728 (m), 736 (m), 752 (m), 827 (w), 889 (w), 1029 (m), 1069 (m), 1188 (m), 1214 (m), 1241 (m), 1270 (m), 1297 (m), 1324 (w), 1345 (w), 1383 (m), 1427 (m), 1471 (s), 1618 (w), 2635 (w), 2850 (s), 2918 (s), 2956 (s). The colorless filtrate was transferred to a 20 mL scintillation vial and the volatiles were removed *in vacuo* to yield a colorless oil (402 mg). The oil was analyzed via ^{1}H NMR spectroscopy, which revealed the presence of unreacted 1-docdecanethiol and di(1-dodecane)disulfide (Figure S8). ^{1}H NMR (400 MHz, 25 °C, CD_2Cl_2): δ 2.68 (t, J_{HH} = 6 Hz, di(1-dodecane)disulfide, α-CH_2), 2.51 (m, 1-dodecanethiol, α-CH_2), 1.66 (m, di(1-dodecane)disulfide, β-CH_2), 1.59 (m, 1-dodecanethiol, β-CH_2), 1.37 (br m, overlapping CH_2 of di(1-dodecane)disulfide and 1-dodecanethiol), 1.27 (br m, overlapping CH_2 of di(1-dodecane)disulfide and 1-dodecanethiol), 0.88 (m, overlapping CH_3 of di(1-dodecane)disulfide and 1-dodecanethiol).

Synthesis of $[Cu_{12}(SR')_6Cl_{12}][(Cu(HSR'))_6]$ (R' = ^{n}Bu) (2). To a stirring slurry of $CuCl_2$ (100.0 mg, 0.744 mmol) in THF (2 mL) was added 1-butanethiol (0.40 mL, 3.71 mmol) via syringe. The brown powder quickly dissolved over the course of 30 s to give a bright yellow solution. The reaction mixture was allowed to stir for 20 min, whereupon it was filtered through a Celite column supported on glass wool (0.5 × 1 cm). The column was washed with THF (1 mL) and the washings were added to the filtrate. The filtrate was then layered with pentane (12 mL) and stored at -25 °C for 2 d, which resulted in the deposition of pale yellow crystals. The crystals were isolated by decanting the supernatant and then dried *in vacuo* to yield **2** (104 mg, 90% yield). Anal. Calcd for $C_{48}H_{114}Cl_{12}Cu_{18}S_{12}$: C, 21.79; H, 4.34. Found C, 23.12; H 4.72. ^{1}H NMR (500 MHz, 25 °C, THF-d_8): δ 3.26 (br s, 12H, SCH_2CH$_2$CH$_2$CH$_3$), 2.53, (br s, 12H, HSCH_2CH$_2$CH$_2$CH$_3$), 1.98 (br s, 12H,

$SCH_2CH_2CH_2CH_3$), 1.85 (br s, 6H, $HSCH_2CH_2CH_2CH_3$), 1.58 (m, 12H, $HSCH_2CH_2CH_2CH_3$), 1.41 (m, 24H, $SCH_2CH_2CH_2CH_3$, overlapping with $HSCH_2CH_2CH_2CH_3$), 0.92 (m, 36H, $SCH_2CH_2CH_2CH_3$, overlapping with $HSCH_2CH_2CH_2CH_3$). ESI-MS: *m/z* = 2139.7942 $[Cu_{18}(SR')_6Cl_{13}]^-$ (Calcd *m/z* = 2139.5649), *m/z* = 2039.9023 $[Cu_{17}(SR')_6Cl_{12}]^-$ (Calcd *m/z* = 2039.6666), *m/z* = 1940.9977 $[Cu_{16}(SR')_6Cl_{11}]^-$ (calcd *m/z* = 1940.7682), *m/z* = 1842.0930 $[Cu_{15}(SR')_6Cl_{10}]^-$ (calcd *m/z* = 1841.8719), *m/z* = 1744.175 $[Cu_{14}(SR')_6Cl_9]^-$ (calcd *m/z* = 1743.9734). UV-Vis / NIR (THF, 21.2 μM, 25 °C, $L \cdot mol^{-1} \cdot cm^{-1}$): 274 nm (sh, ε = 44000), 370 nm (ε = 22000). Fluorescence (λ_{ex} = 365 nm): 585 nm (FWHM = 140 nm). IR (KBr pellet, cm^{-1}): 649 (w), 705 (m), 728 (m), 780 (w), 914 (m), 1052 (m), 1068 (m), 1222 (s), 1270 (m), 1298 (m), 1337 (w), 1353 (w), 1379 (m), 1429 (m), 1463 (s), 1618 (w), 2502 (w), 2646 (w), 2731 (w), 2872 (s), 2928 (s), 2957 (s). Complex **2** could also be prepared, in similar yields, by using dibenzyl ether as the solvent.

Synthesis of di-*n*-butyl disulfide. To a stirring slurry of colorless Na(S^{n}Bu) (69 mg, 0.615 mmol) in THF (5 mL) was added dropwise a THF solution (2 mL) of I_2 (78 mg, 0.307 mmol) over the course of 10 min. The reaction mixture was allowed stir for 20 h, whereupon the volatiles were removed *in vacuo* and the resulting colorless oil was triturated with pentane (3 × 2 mL) to remove any remaining THF. The volatiles were then removed *in vacuo* to give di-*n*-butyl disulfide as a colorless oil (48 mg, 87% yield). ^{1}H NMR (500 MHz, 25 °C, CD_2Cl_2): δ 2.69 (t, J_{HH} = 5 Hz, 4H, $SCH_2CH_2CH_2CH_3$), 1.65 (m, 4H, $SCH_2CH_2CH_2CH_3$), 1.41 (m, 4H, $SCH_2CH_2CH_2CH_3$), 0.92 (t, J_{HH} = 7 Hz, 6H, $SCH_2CH_2CH_2CH_3$). ^{13}C NMR (125 MHz, 25 °C, CD_2Cl_2): δ 39.28 ($SCH_2CH_2CH_2CH_3$), 31.76 ($SCH_2CH_2CH_2CH_3$), 22.08 ($SCH_2CH_2CH_2CH_3$), 13.89 ($SCH_2CH_2CH_2CH_3$). GC-MS: *m/z* = 178.07 $[M]^+$ (Calcd *m/z* = 178.08). These NMR spectral data are similar to those previously reported for di-*n*-butyl disulfide in $CDCl_3$.[7]

Reaction of 2 with pyridine. A 20 mL scintillation vial was charged with a magnetic stir bar, complex **2** (17.7 mg, 6.69 μmol), and pyridine (2.0 mL, 25 mmol). The pale yellow solid quickly dissolved to give a bright yellow solution. The solution was allowed to stir for 20 min, whereupon a small amount of white powder deposited from solution. The reaction mixture was then filtered through a Celite column supported on glass wool (0.5 × 1 cm). The column was washed with pyridine (1 mL) and the washings were added to the filtrate. The filtrate was then layered with diethyl ether (12 mL) and stored at room temperature for 2 d, which resulted in the deposition of yellow needles. The crystals were isolated by decanting the supernatant and then dried *in vacuo* to yield [$CuCl(py)_3$] (18.3 mg, 68% yield based on Cl^-). The identity of the crystals was confirmed by a comparison of the unit cell parameters with the literature values.[8] Unit cell parameters: a = 14.353(2) Å, b = 9.833(2) Å, 11.710 (2) Å; α= 90.00°, β = 90.00°, γ = 90.00°.

Synthesis of $[H(THF)_2]_2[Cu_{17}(SR")_6Cl_{13}(THF)_2(HSR")_3]$ (R" = CH_2CH_2Ph) (3). To a stirring slurry of $CuCl_2$ (90.0 mg, 0.692 mmol) in THF (2 mL) was added 2-phenylethanethiol (0.36 mL, 2.69 mmol) via syringe. The brown powder quickly dissolved over the course of 30 s to give a bright yellow solution. The reaction mixture was allowed to stir for 20 min, whereupon it was filtered through a Celite column supported on glass wool (0.5 × 1 cm). The column was washed with THF (1 mL) and the washings were added to the filtrate. The filtrate was then layered with pentane (12 mL) and stored at -25 °C for 2 d, which resulted in the deposition of pale yellow crystals. The crystals were isolated by decanting the supernatant and then dried *in vacuo* to yield **3** (113 mg, 94%). Anal. Calcd for $C_{96}H_{136}Cl_{13}Cu_{17}O_6S_9$: C, 35.86; H, 4.26. Found C, 37.93; H 4.60. ^{1}H NMR (400 MHz, 25 °C, THF-d_8): δ 8.82 (br s, 2H, $[H(THF)_2]^+$), 7.31-7.15 (m, 45H, overlapping phenyl peaks of SCH_2CH_2Ph and $HSCH_2CH_2Ph$), 3.47 (m, 12H, SCH_2CH_2Ph), 3.37 (m, 12H, SCH_2CH_2Ph), 2.88 (m, 6H, $HSCH_2CH_2Ph$), 2.77 (m, 6H, $HSCH_2CH_2Ph$), 1.95 (br s, 3H,

*H*SCH$_2$CH$_2$Ph). ESI-MS: *m/z* = 2527.6428 [Cu$_{19}$(SR")$_6$Cl$_{14}$]$^-$ (Calcd *m/z* = 2527.4636), *m/z* = 2431.7378 [Cu$_{18}$(SR")$_6$Cl$_{13}$]$^-$ (Calcd *m/z* = 2431.5574), *m/z* = 2327.6748 [Cu$_{17}$(SR")$_6$Cl$_{12}$]$^-$ (calcd *m/z* = 2327.6667), *m/z* = 2229.7747 [Cu$_{16}$(SR")$_6$Cl$_{11}$]$^-$ (Calcd *m/z* = 2229.7683), *m/z* = 2129.8726 [Cu$_{15}$(SR")$_6$Cl$_{10}$]$^-$ (Calcd *m/z* = 2129.8718), *m/z* = 2031.9645 [Cu$_{14}$(SR")$_6$Cl$_9$]$^-$ (Calcd *m/z* = 2031.9734), *m/z* = 1932.0714 [Cu$_{13}$(SR")$_6$Cl$_8$]$^-$ (Calcd *m/z* = 1932.0750), *m/z* = 1831.0859 [Cu$_{12}$(SR")$_6$Cl$_7$]$^-$ (Calcd *m/z* = 1831.1843). UV-Vis / NIR (THF, 24.4 μM, 25 °C, L·mol^{-1}·cm^{-1}): 260 nm (sh, ε = 49000), 355 nm (ε = 15000). Fluorescence (λ_{ex} = 365 nm): 650 nm (FWHM = 190 nm). IR (KBr pellet, cm^{-1}): 493 (m), 565 (m), 647 (w), 706 (s), 756 (s), 846 (w), 909 (w), 969 (m), 1029 (m), 1070 (m), 1222 (m), 1266 (w), 1312 (m), 1417 (m), 1453 (s), 1496 (s), 1583 (w), 1602 (m), 1808 (w), 1878 (w), 1949 (w), 2524 (w), 2632 (w), 2870 (m), 2928 (s), 2026 (s), 3060 (m).

Reaction of 3 with pyridine. A 20 mL scintillation vial was charged with a magnetic stir bar, complex **3** (20.6 mg, 6.41 μmol), and pyridine (2.0 mL, 25 mmol). The pale yellow solid quickly dissolved to give a bright yellow solution. The solution was allowed to stir for 20 min. The reaction mixture was then filtered through a Celite column supported on glass wool (0.5 × 1 cm). The column was washed with pyridine (1 mL) and the washings were added to the filtrate. The filtrate was then layered with diethyl ether (14 mL) and stored at room temperature for 2 d, which resulted in the deposition of yellow needles. The crystals were isolated by decanting the supernatant and then dried *in vacuo* to yield [CuCl(py)$_3$] (26.5 mg, 95% yield based on Cl$^-$). The identity of the crystals was confirmed by a comparison of the unit cell parameters with the literature values.[8] a = 14.340(2) Å, b = 9.828(2) Å, 11.692 (2) Å; α= 90.00°, β = 90.00°, γ = 90.00°.

X-ray Crystallography. Data for **2** were collected on a Bruker APEX 3 D8 diffractometer equipped with a PHOTON II CPAD detector on Beamline 12.2.1 at the Lawrence Berkeley National Laboratory Advanced Light Source (ALS) Synchrotron X-ray source (α = 0.7288 Å),

which operates at 1.9 GeV with a ring current of 500 mA. X-rays were monochromatized using reflection from a Si(111) monochrometer. Data for **3**·1.5THF were collected on a Bruker KAPPA APEX II diffractometer equipped with an APEX II CCD detector using a TRIUMPH monochromater with a MoKα X-ray source (α = 0.71073 Å). Crystals were mounted on a cryoloop under Paratone-N oil, and all data were collected at 100(2) K using an Oxford nitrogen gas cryostream system.

X-ray data for both **2** and **3**·1.5THF were collected utilizing frame exposures of 10 s. Data collection and cell parameter determination was conducted using the SMART program.[9] Integration of the data frames and final cell parameter refinement were performed using SAINT software.[10] Absorption correction of the data was carried out using the multi-scan method SADABS.[11] Subsequent calculations were carried out using SHELXTL.[12] Structure determination was done using direct methods and difference Fourier techniques. All hydrogen atom positions on the ligands were idealized, and rode on the atom of attachment. Structure solution, refinement, graphics, and creation of publication materials were performed using SHELXTL.[12]

For complexes **2** and **3**, hydrogen atoms were not assigned to the thiol (i.e., RSH) sulfur atoms. Additionally, for complex **3**, the H^+ counterions could not be located in the Fourier difference map and were not assigned. Due to unresolved positional disorder, the EADP command was applied to some of the carbon atoms of three thiolate (S2, S3, S4) ligands and one thiol (S8) ligand in **3**. Similarly, the FLAT and DFIX commands were used to constrain the phenyl ring of one thiol ligand in **3**, due to unresolved positional disorder. One THF solvate (O7) was constrained using the DFIX, SADI, and FREE commands. One THF solvate (O6) was modelled with 50% occupancy.

Further crystallographic details can be found in Table S1.

Table S1. X-ray Crystallographic Data for **2** and **3**·1.5THF.

	2	**3**·1.5THF
empirical formula	$C_{48}H_{114}Cl_{12}Cu_{18}S_{12}$	$C_{102}H_{148}Cl_{13}Cu_{17}O_{7.5}S_9$
crystal habit, color	needle, pale yellow	block, pale yellow
crystal size (mm)	0.050 0.015 0.005	0.2 0.2 0.15
crystal system	triclinic	triclinic
space group	$P\bar{1}$	$P\bar{1}$
volume ($Å^3$)	2185.8(4)	6439(12)
a (Å)	12.5832(13)	15.268(15)
b (Å)	13.4715(13)	15.916(18)
c (Å)	14.9134(14)	29.58(3)
α (deg)	60.640(4)	91.56(2)
β (deg)	86.533(5)	101.67(2)
γ (deg)	73.574(4)	111.83(2)
Z	1	2
formula weight (g/mol)	2645.23	3323.77
density (calculated) (Mg/m^3)	2.010	1.700
absorption coefficient (mm^{-1})	5.306	3.178
F_{000}	1320	3356
total no. reflections	11797	25756
unique reflections	8613	12659
final R indices [I>2σ(I)]	$R_1 = 0.0525$	$R_1 = 0.0849$
	$wR_2 = 0.1133$	$wR_2 = 0.2046$
largest diff. peak and hole (e^-A^{-3})	1.915 and -1.717	2.343 and -1.524
GOF	1.390	1.224

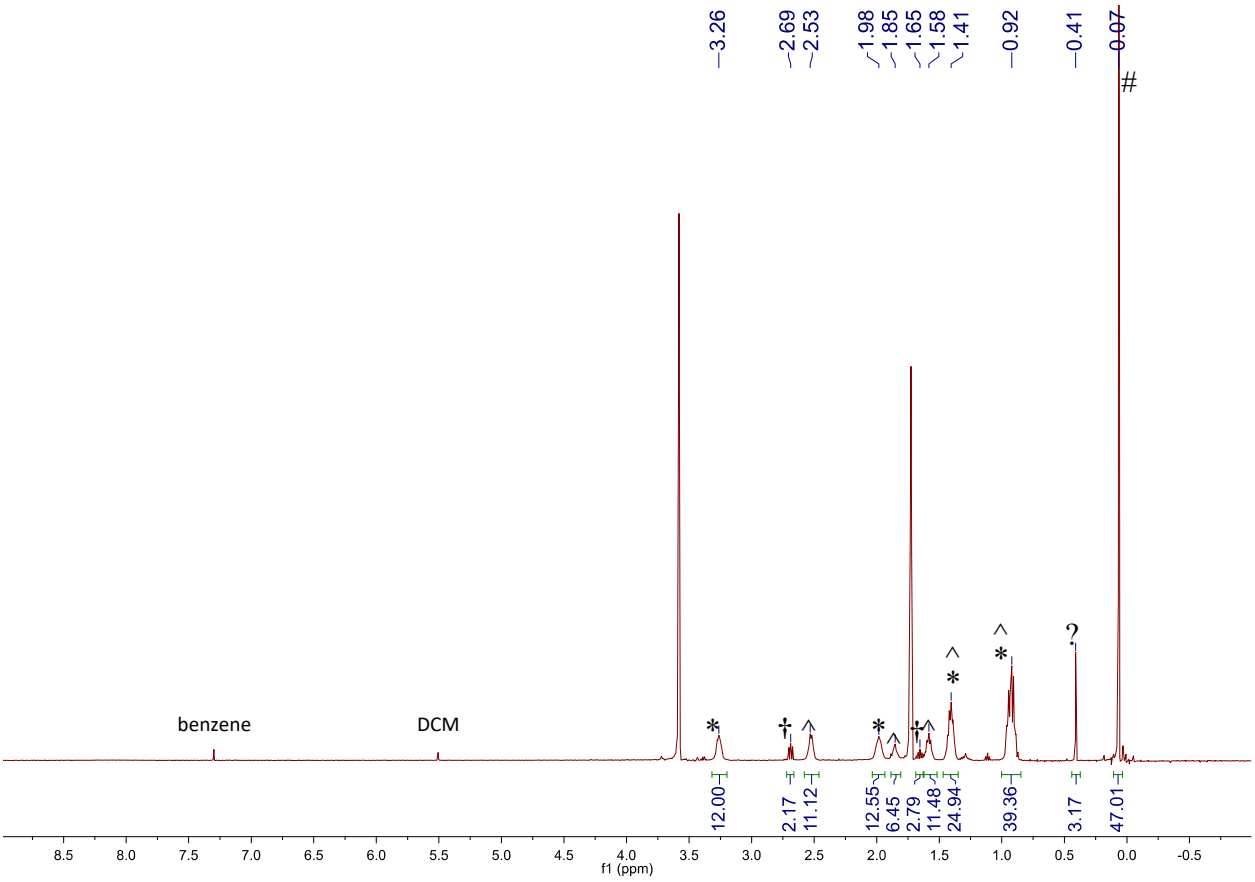

Figure S1. ^{1}H NMR spectrum of **2** in THF-*d*$_8$ with HMDSO added as an internal standard. **Experimental details:** Complex **2** (8.0 mg, 3.0 µmol) was transferred to a J. Young NMR tube equipped with a rotoflow Teflon valve and dissolved in THF-*d*$_8$ (1 mL). HMDSO (1.0 µL, 4.7 µmol) was added via syringe as an internal standard. A ^{1}H NMR spectrum was then collected using a long relaxation delay (d_1 = 60 s) to ensure accurate integrations. (*) indicates a resonance assignable to **2**, (^) indicates a resonance assignable to HS^{n}Bu, (†) indicates a resonance assignable to di-*n*-butyl disulfide, (#) indicates a resonance assignable to HMDSO, and (?) indicates a resonance assignable to an unknown impurity.

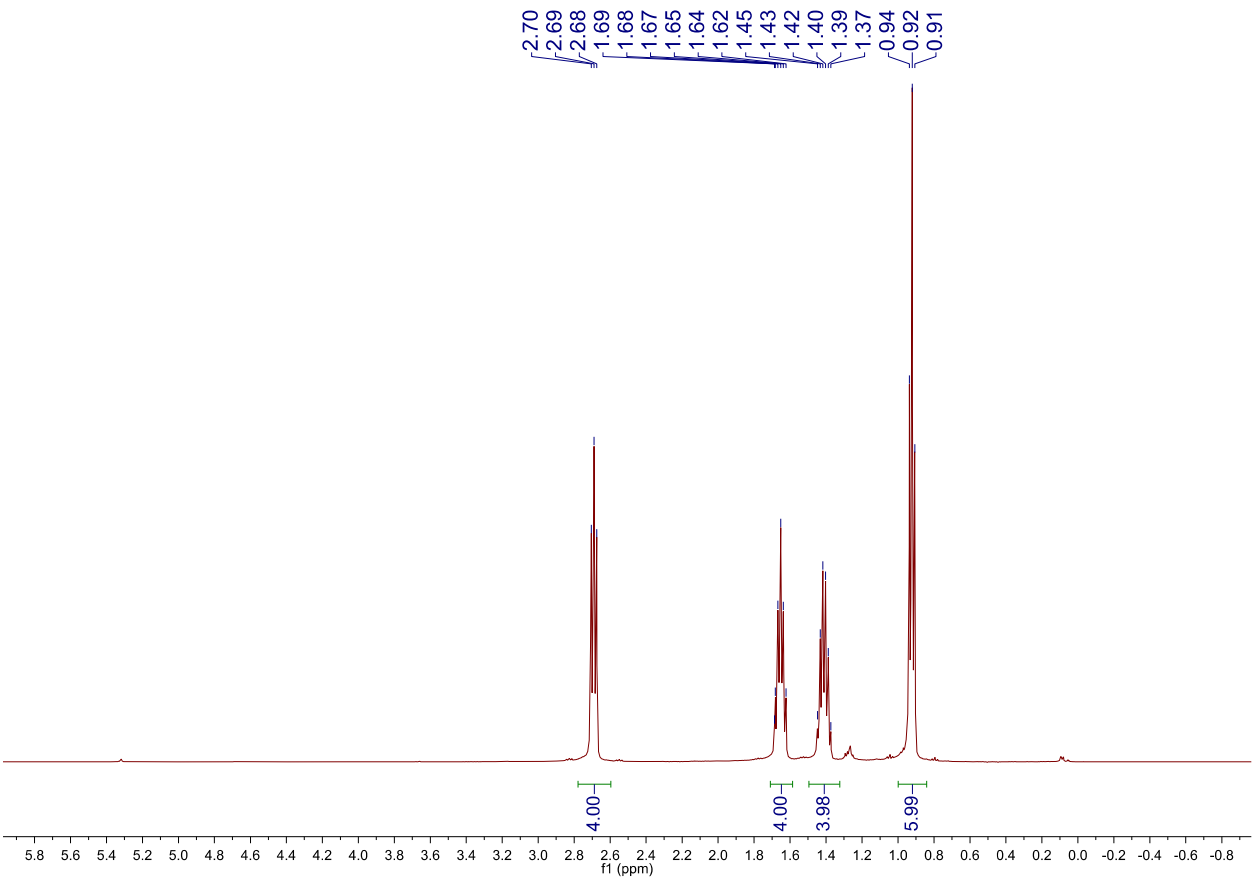

Figure S2. ^{1}H NMR spectrum of di-*n*-butyl disulfide in CD_2Cl_2.

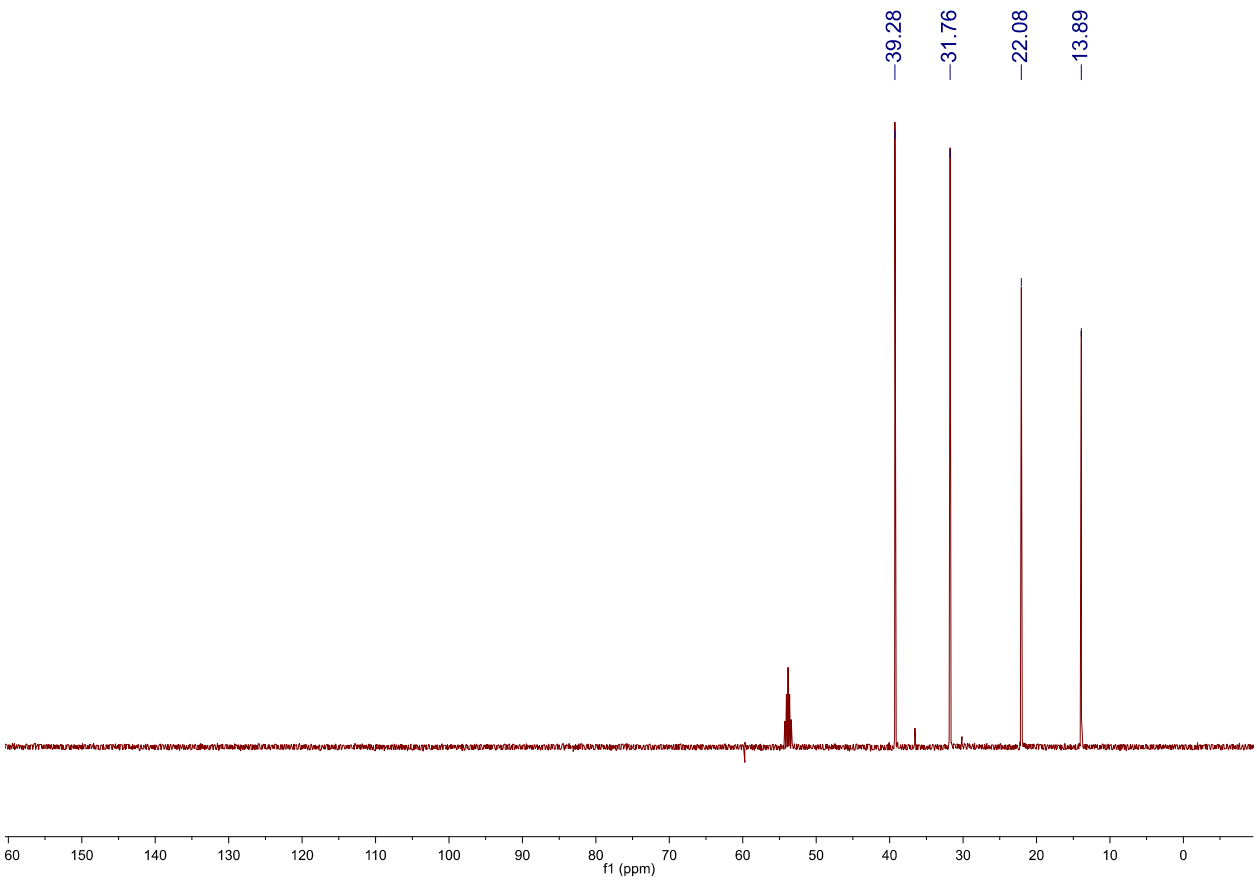

Figure S3. ^{13}C NMR spectrum of di-*n*-butyl disulfide in CD_2Cl_2.

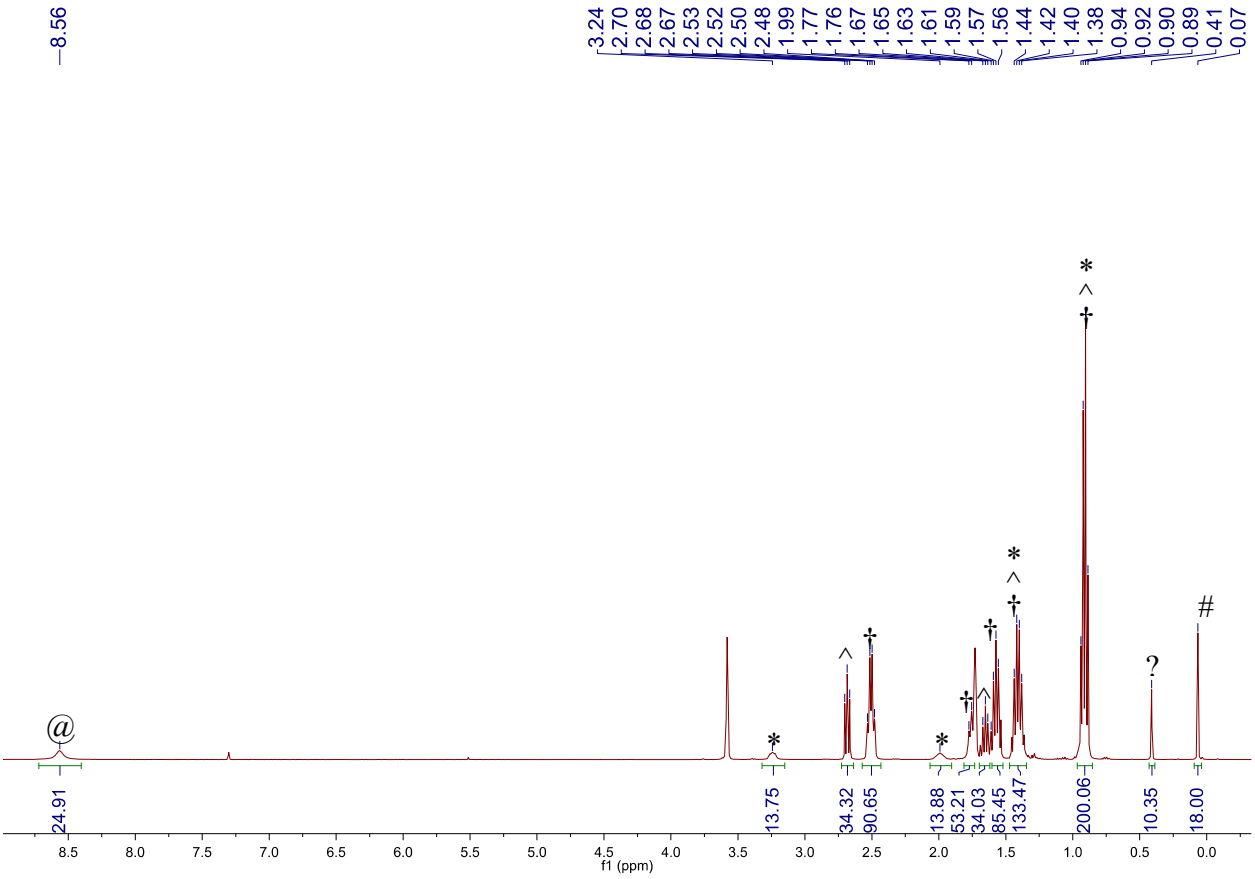

Figure S4. *In situ* ^{1}H NMR spectrum in THF-d_8 of the reaction of $CuCl_2$ and HS^{n}Bu after 20 min. **Experimental details:** $CuCl_2$ (6 mg, 0.045 mmol) was added to a J. Young NMR tube equipped with a rotoflow Teflon valve and suspended in THF-d_8 (0.8 mL). To this suspension was added HS^{n}Bu (25 µL, 0.23 mmol), whereupon the brown solids dissolved and a bright yellow solution was formed. To this reaction mixture was added HMDSO (0.5 µL, 2.35 µmol) via syringe as an internal standard. The J. Young tube was allowed to stand for 20 min, whereupon a ^{1}H NMR spectrum was collected with a long relaxation delay (d_1 = 60 s) to ensure accurate integrations. (*) indicates resonances assignable to **2**, (^) indicates a resonance assignable to di-*n*-butyl disulfide, (†) indicates a resonance assignable to 1-butanethiol, (@) indicates a resonance assignable to HCl, (#) indicates a resonance assignable to HMDSO, and (?) indicates a resonance assignable to an unidentified side-product.

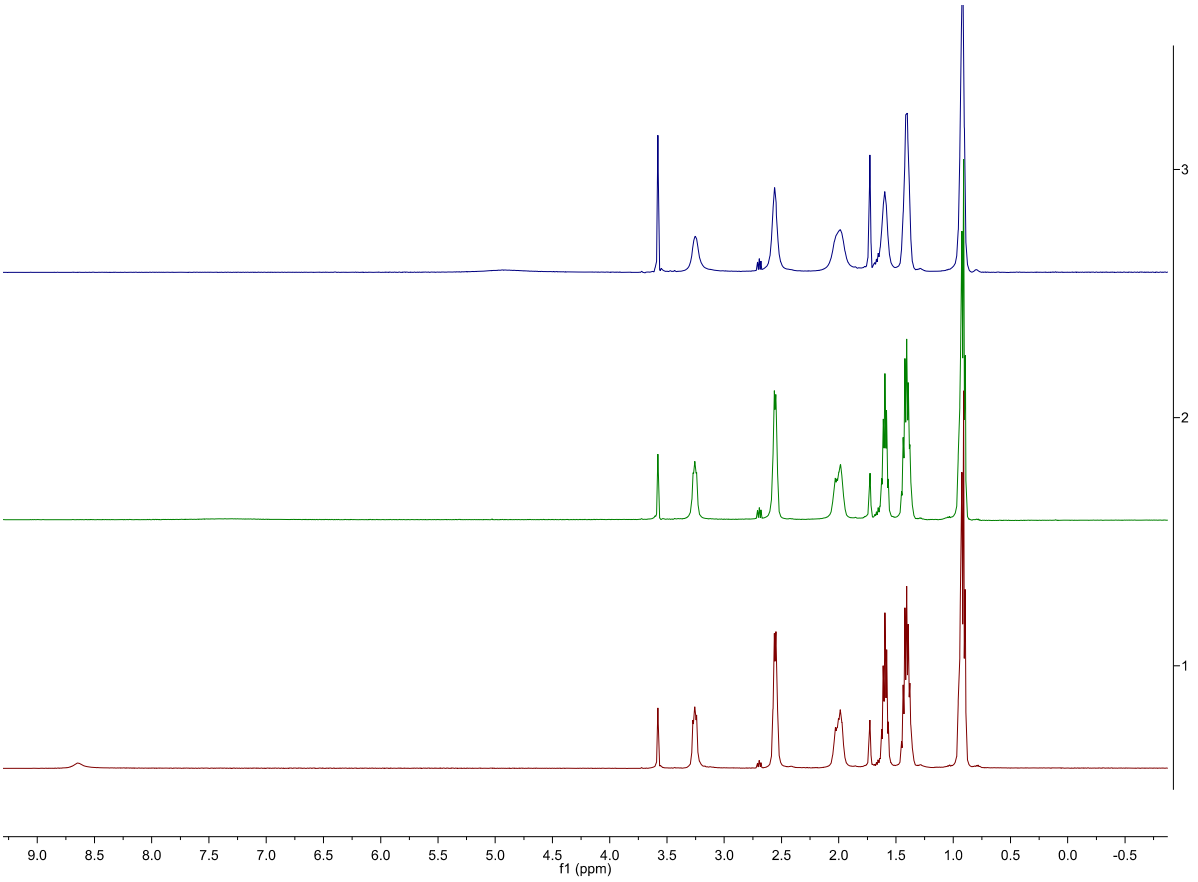

Figure S5. ^{1}H NMR spectra of **2** in THF-d_8 at 25 °C over a period of 24 h. Bottom = 10 min, middle = 5 h, top = 24 h.

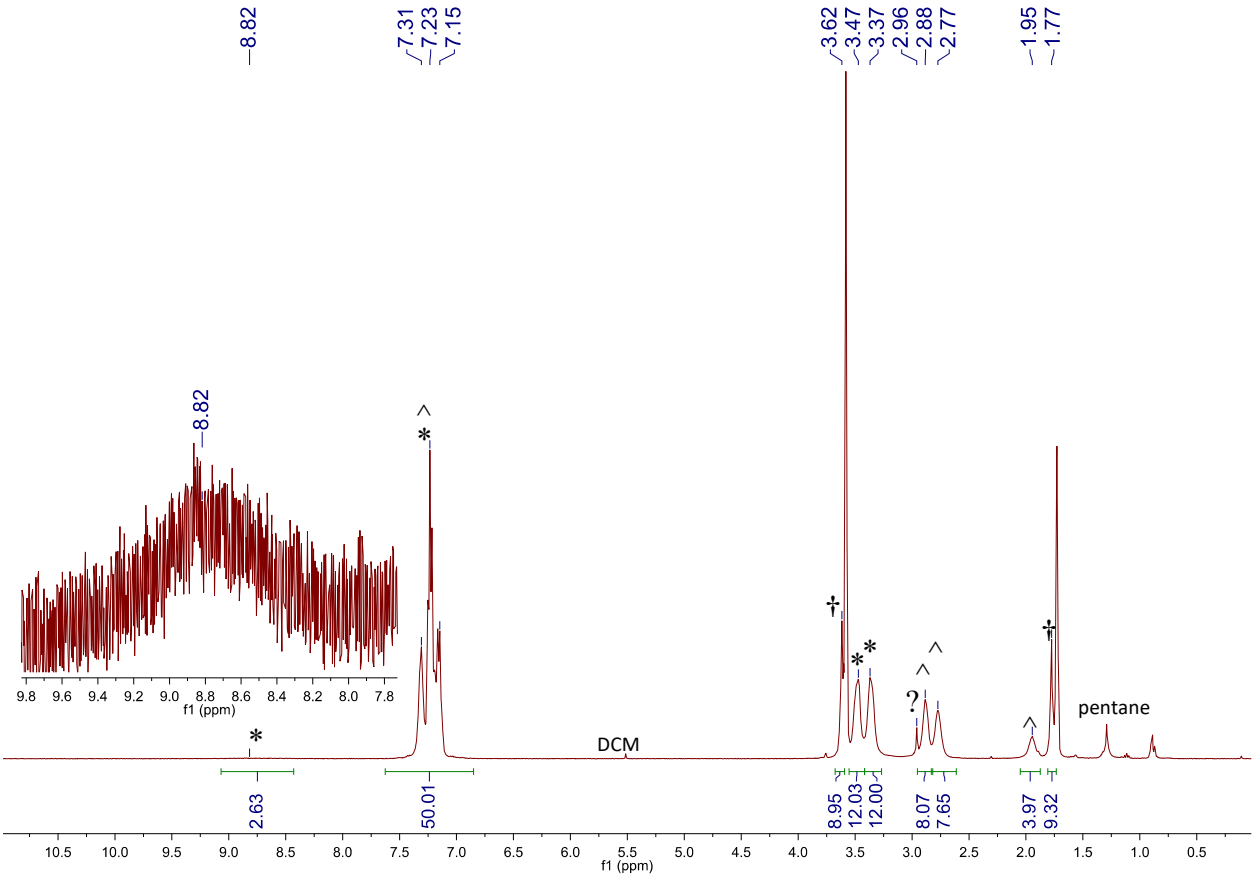

Figure S6. ^{1}H NMR spectrum of **3** in THF-d_8 with an inset showing the H-bonded proton resonance of the $[H(THF)_2]^+$ cation. (*) indicates resonances assignable to **3**, (^) indicates a resonance assignable to $HSCH_2CH_2Ph$, (†) indicates a resonance assignable to THF, and (?) indicates a resonance assignable to an unknown impurity.

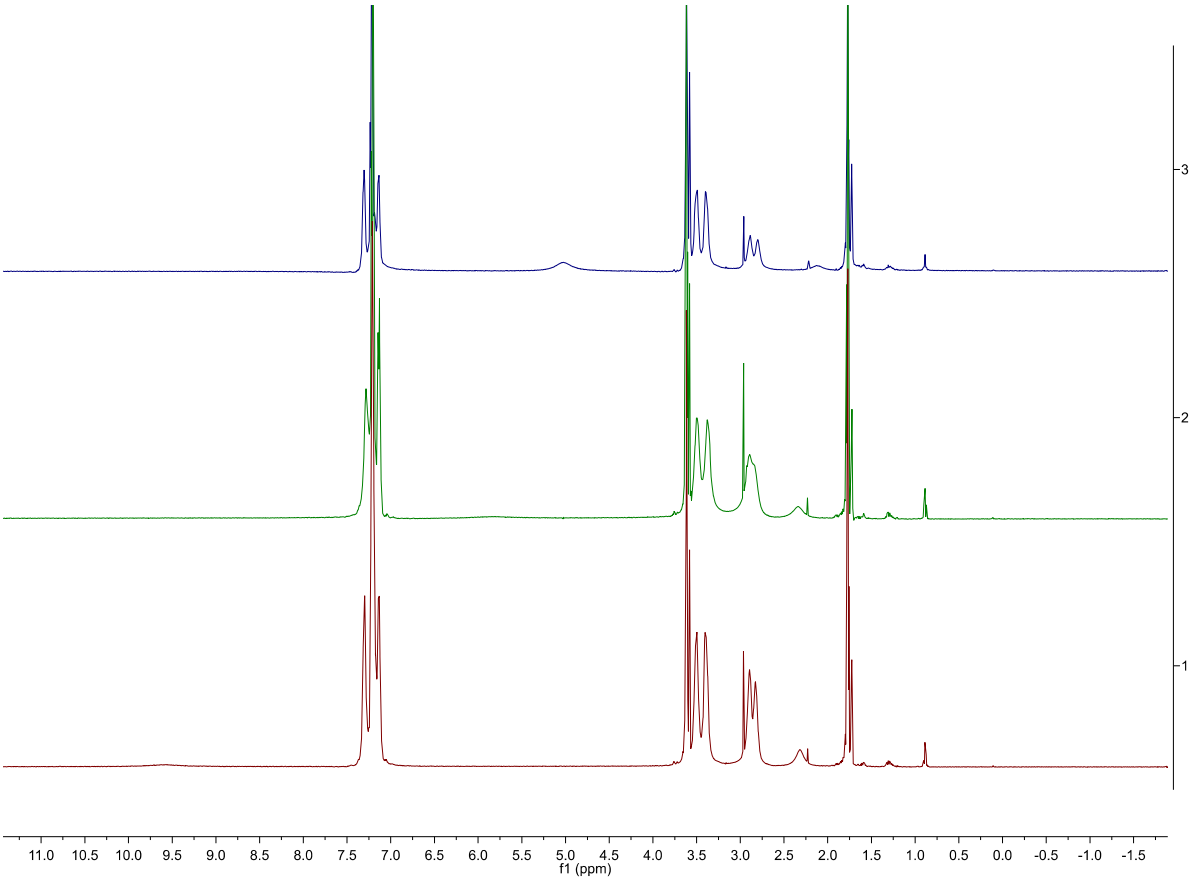

Figure S7. ^{1}H NMR spectra of **3** in THF-*d*$_8$ at 25 °C over a period of 24 h. Bottom = 10 min, middle = 5 h, top = 24 h.

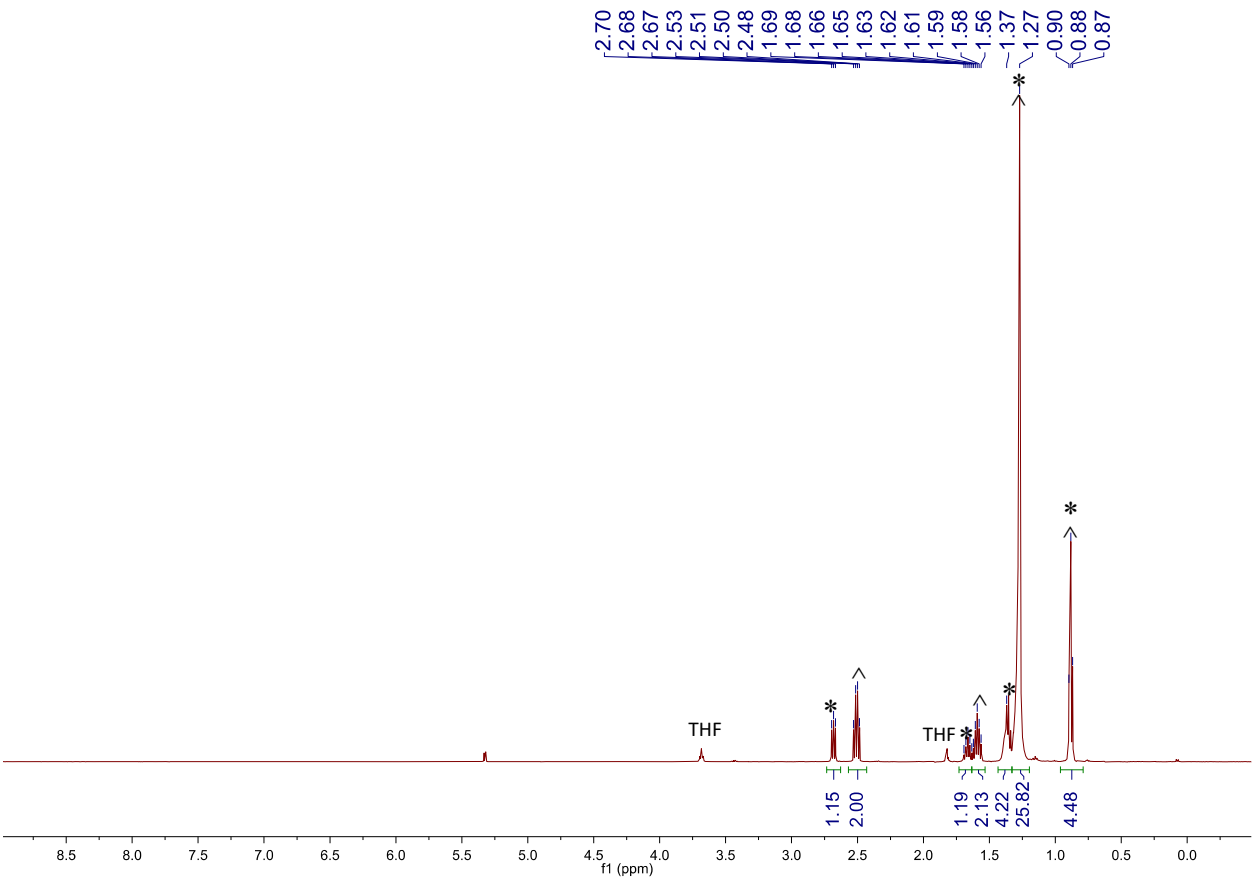

Figure S8. ^{1}H NMR spectrum in CD_2Cl_2 of the THF soluble products from the reaction of $CuCl_2$ and 1-dodecanethiol. (*) indicates a resonance assignable to di(1-dodecane)disulfide[13] and (^) indicates a resonance assignable to 1-dodecanethiol.

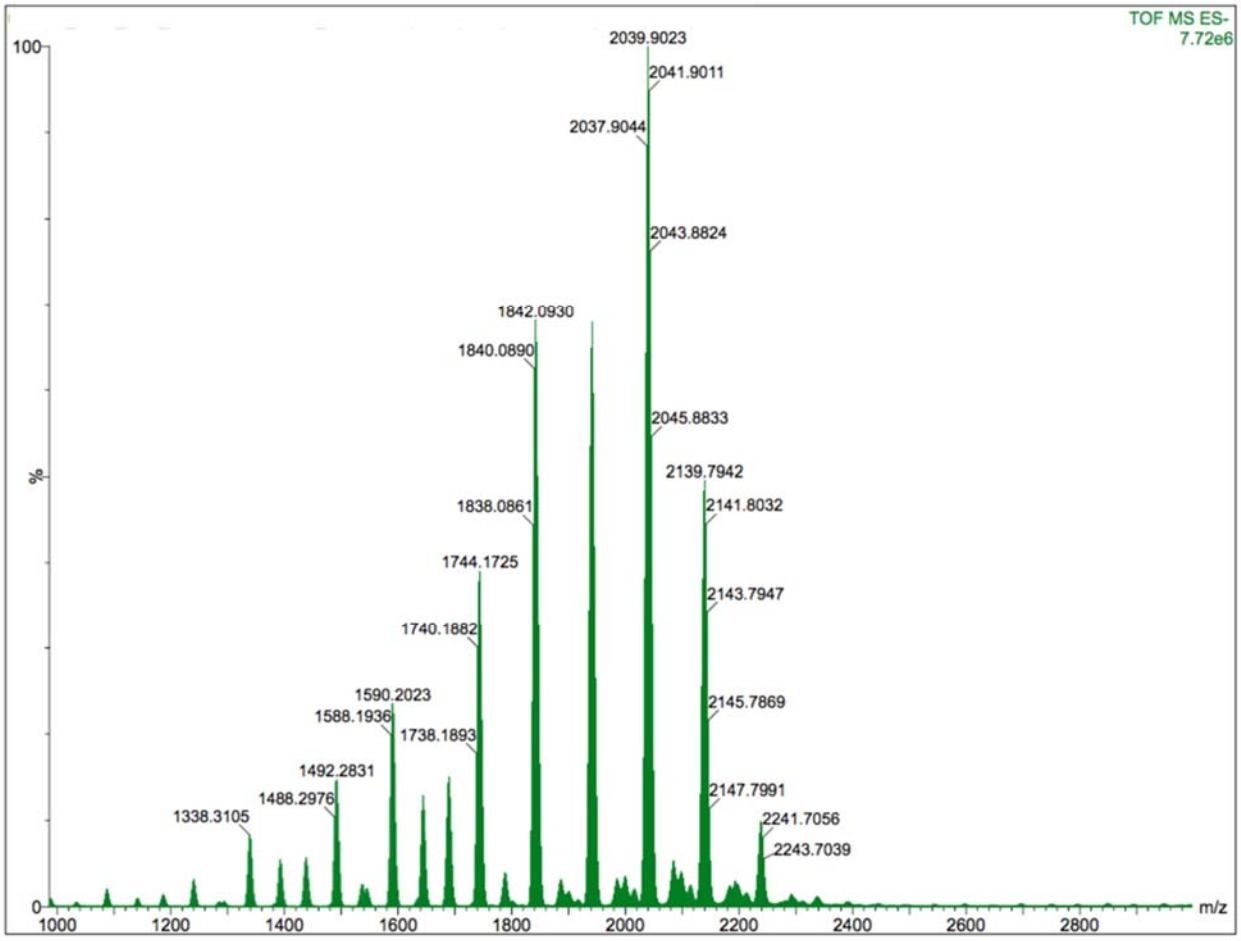

Figure S9. Partial ESI-MS (negative mode) of **2** in THF with added [NEt_4][Cl]. The parent peak at *m/z* = 2039.9023 represents $[Cu_{17}(SR')_6Cl_{12}]^-$ (R' = ^{n}Bu). The surrounding peaks are related to the parent ion by ±$[CuCl]_n$.

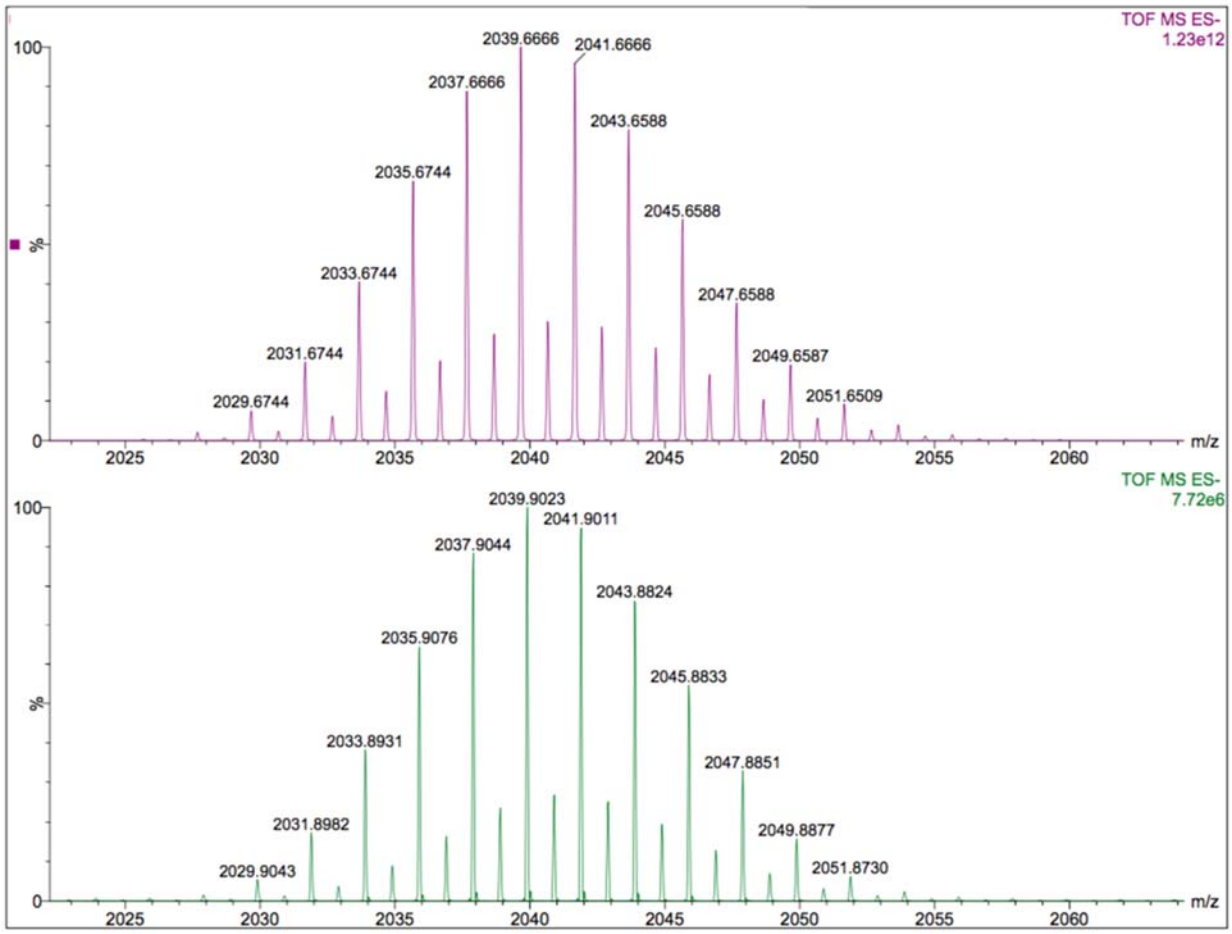

Figure S10. Partial ESI-MS (negative mode) of **2** in THF with added [NEt$_4$][Cl]. The experimental (bottom) and calculated (top) peaks assignable to the $[Cu_{17}(SR')_6Cl_{12}]^-$ (R' = ^{n}Bu) ion are shown.

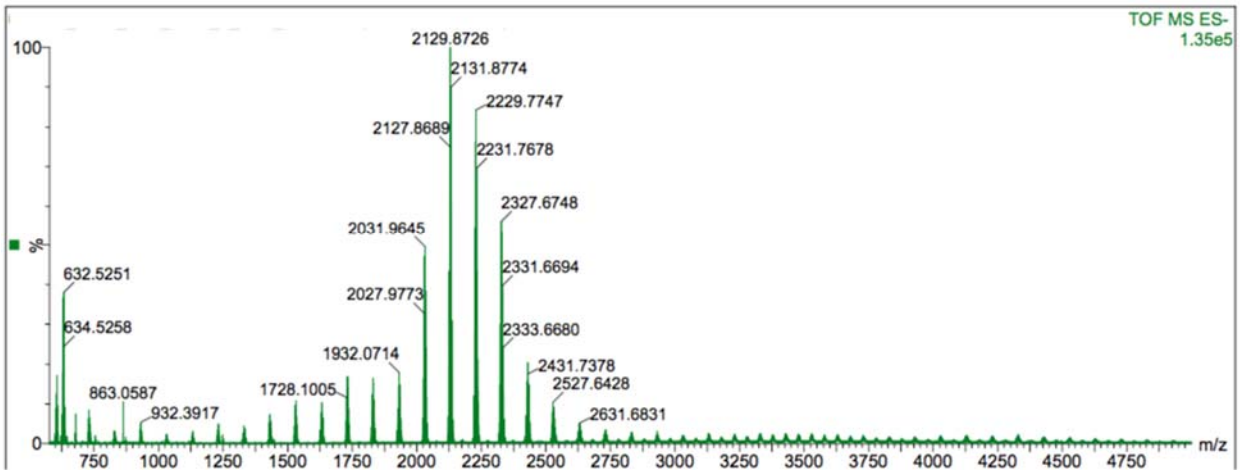

Figure S11. Partial ESI-MS (negative mode) of **3** in THF with added [NEt4][Cl]. The parent peak at *m/z* = 2129.8726 represents $[Cu_{15}(SR")_6Cl_{10}]^-$ (R" = CH_2CH_2Ph). The surrounding peaks are related to the parent ion by ±$[CuCl]_n$.

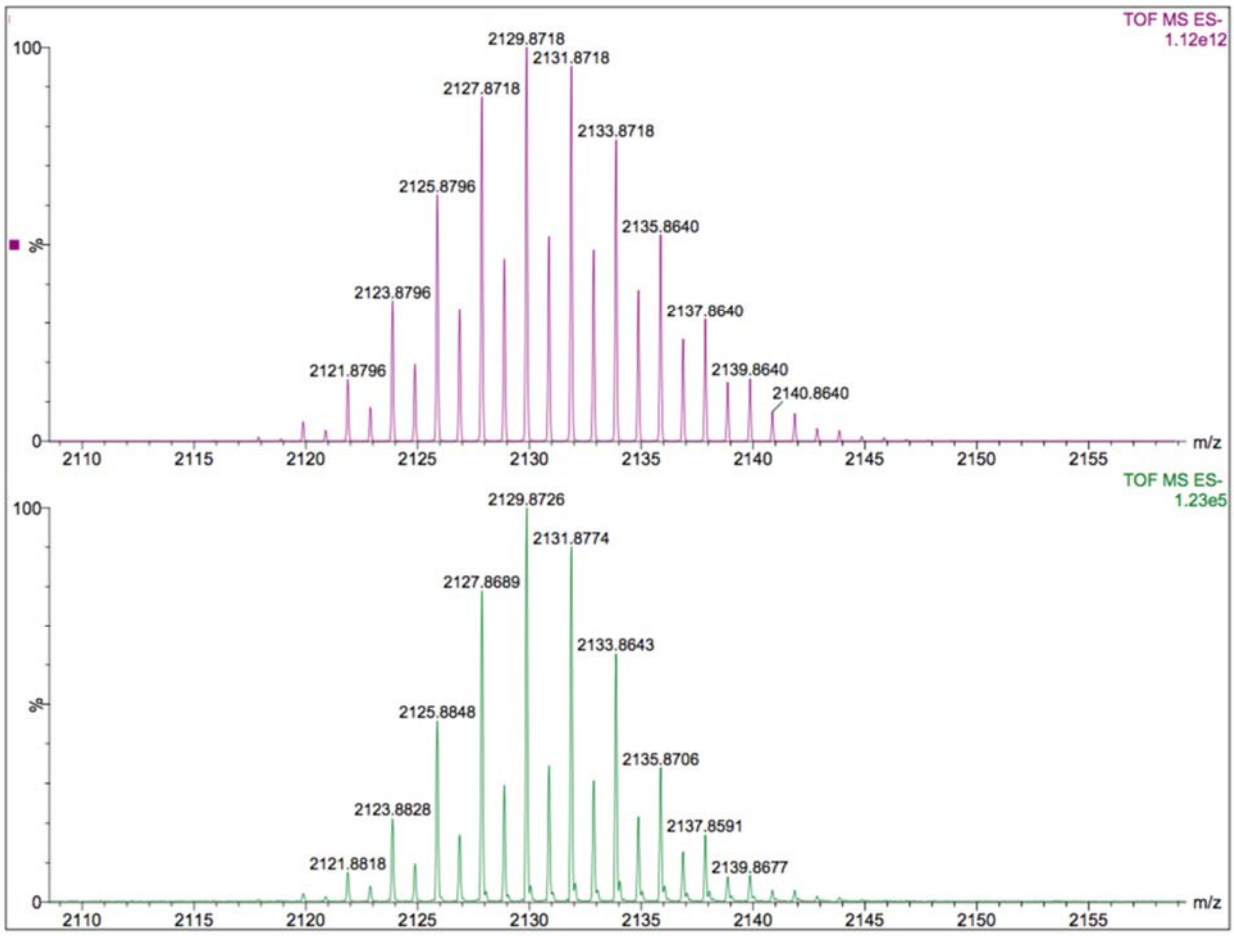

Figure S12. Partial ESI-MS (negative mode) of **3** in THF with added [NEt_4][Cl]. The experimental (bottom) and calculated (top) peaks assignable to the $[Cu_{15}(SR")_6Cl_{10}]^-$ (R" = CH_2CH_2Ph) ion are shown.

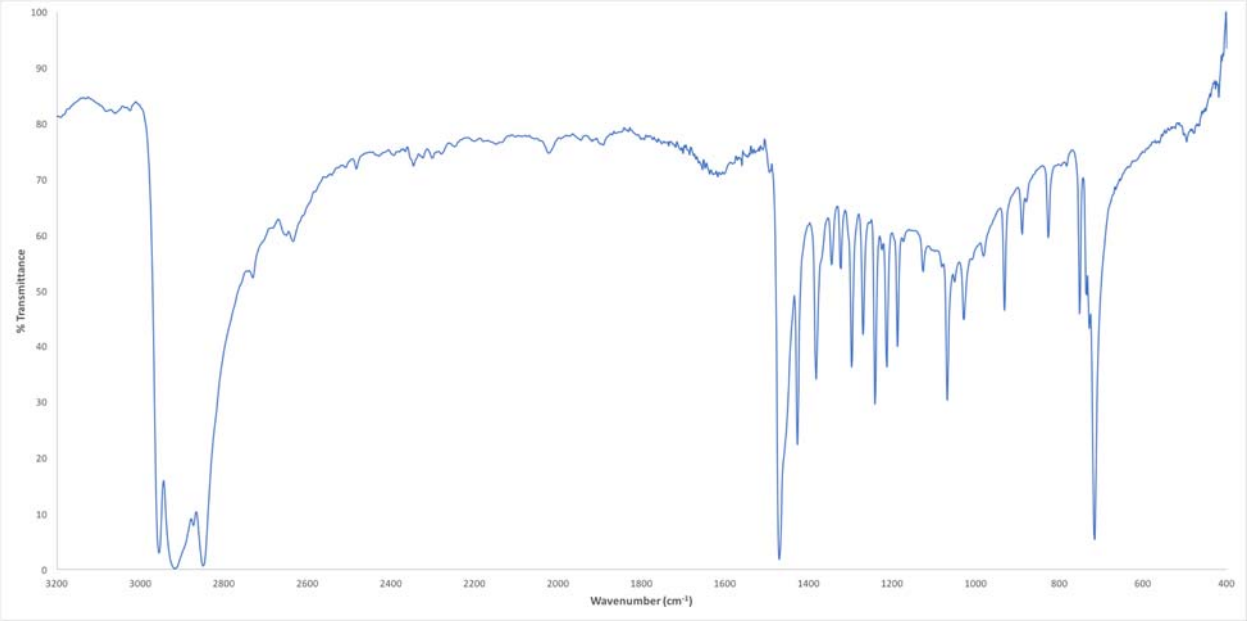

Figure S13. Partial IR spectrum of **1**, synthesized from THF (KBr pellet).

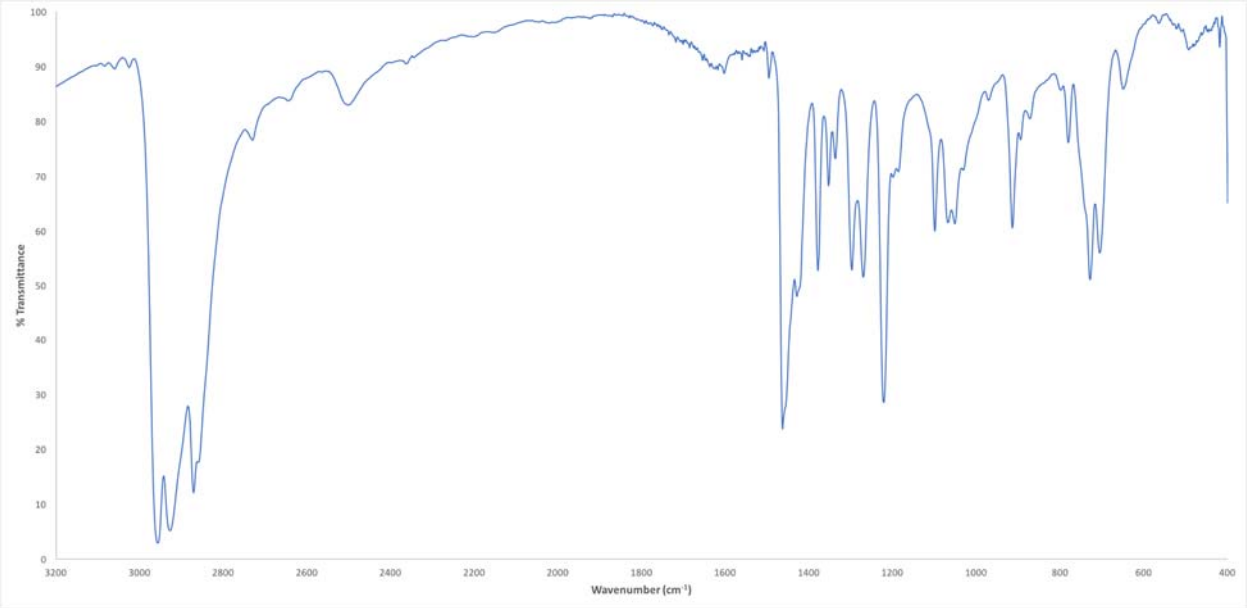

Figure S14. Partial IR spectrum of **2** (KBr pellet).

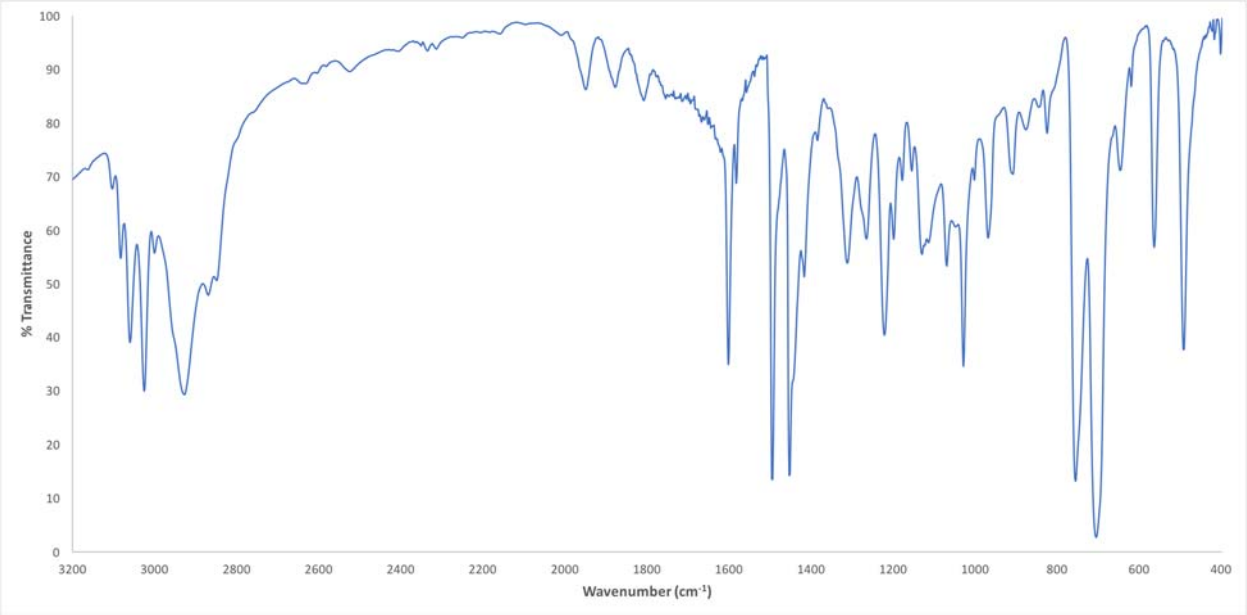

Figure S15. Partial IR spectrum of **3** (KBr pellet).

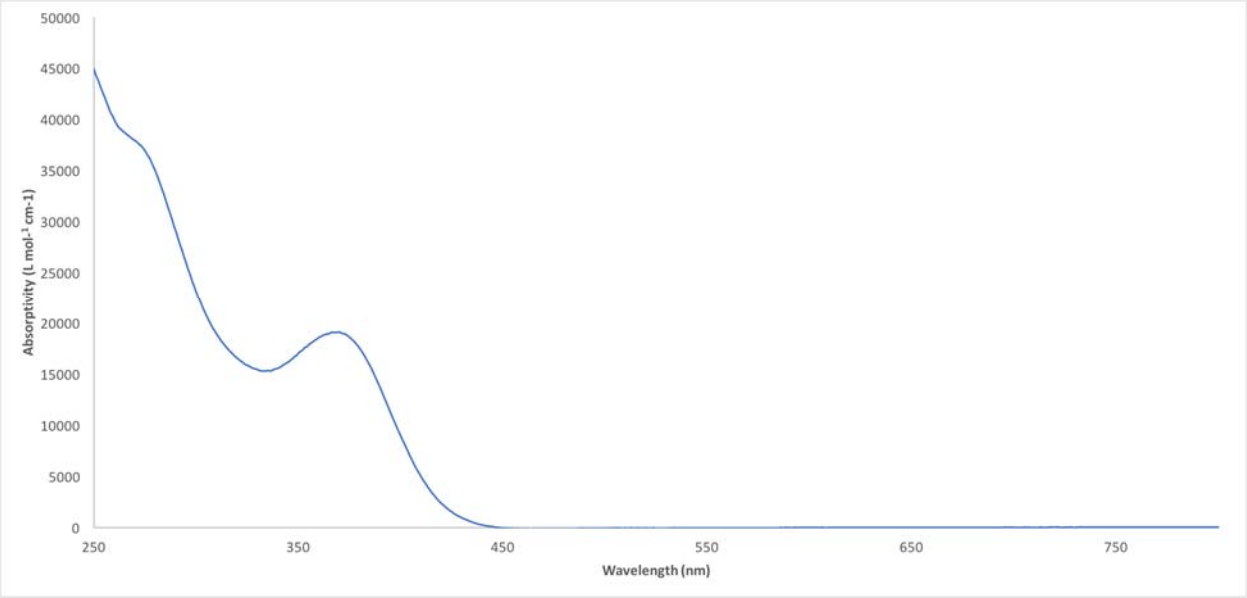

Figure S16. UV / Vis spectrum of **2** (21.2 μM) in THF.

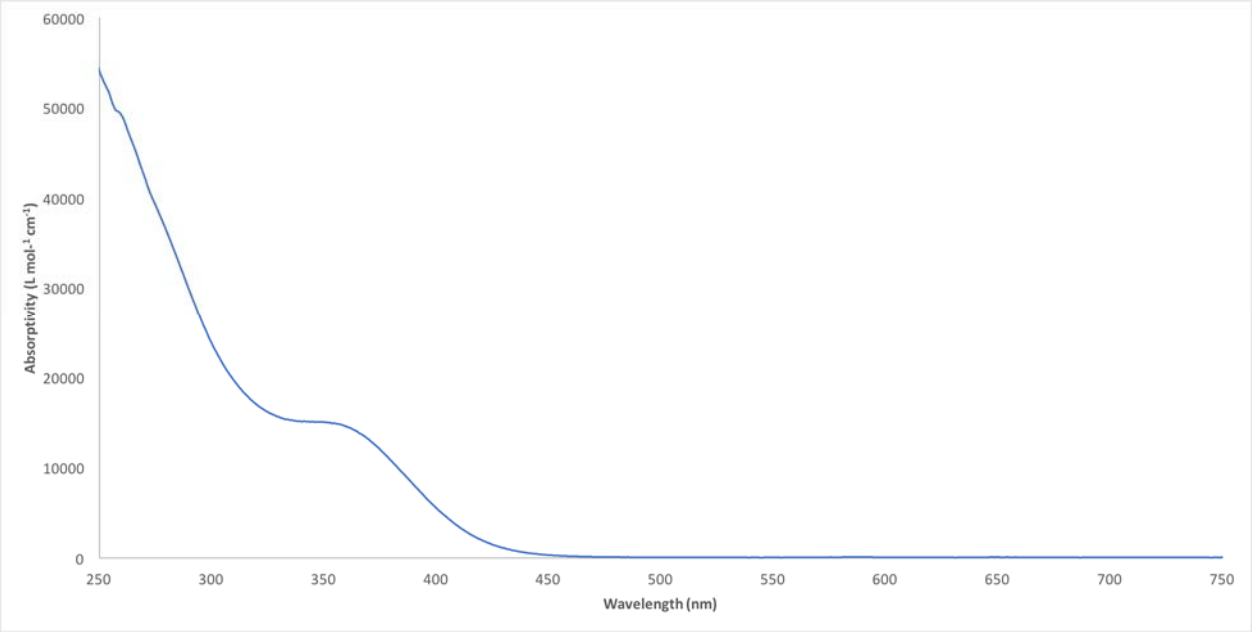

Figure S17. UV / Vis spectrum of **3** (24.4 μM) in THF.

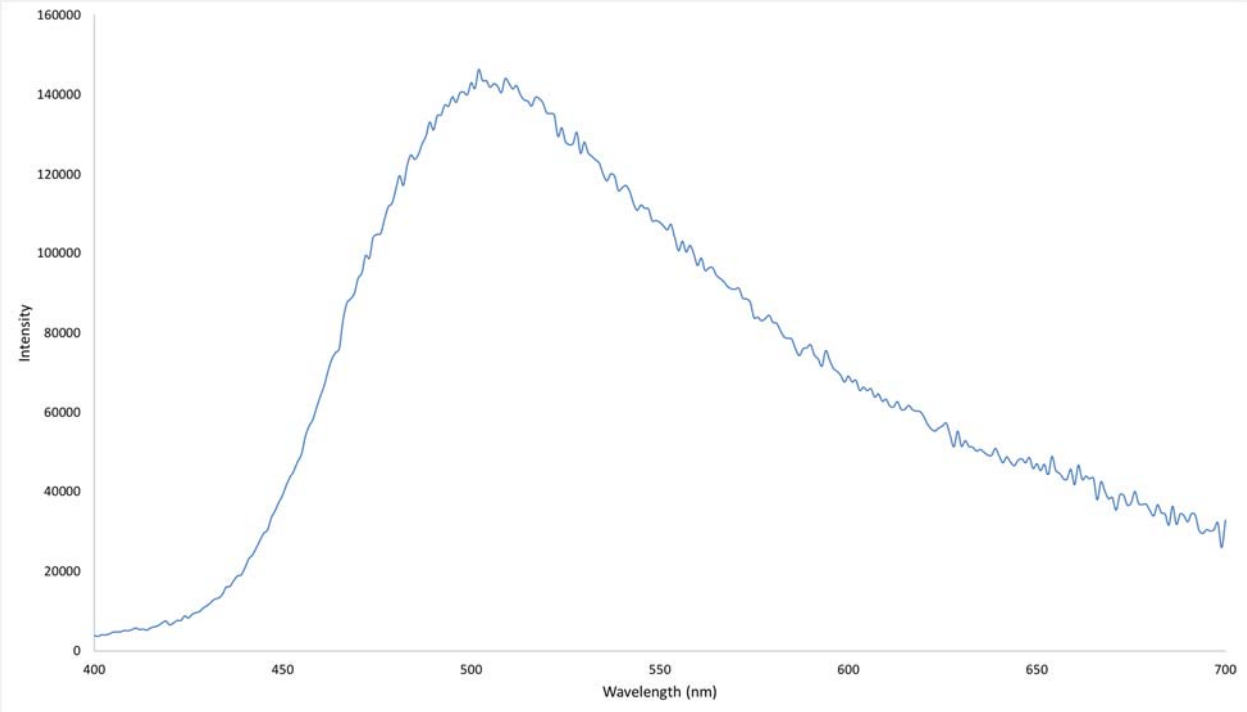

Figure S18. Emission spectrum taken of solid **1**, synthesized from THF, excited at 365 nm.

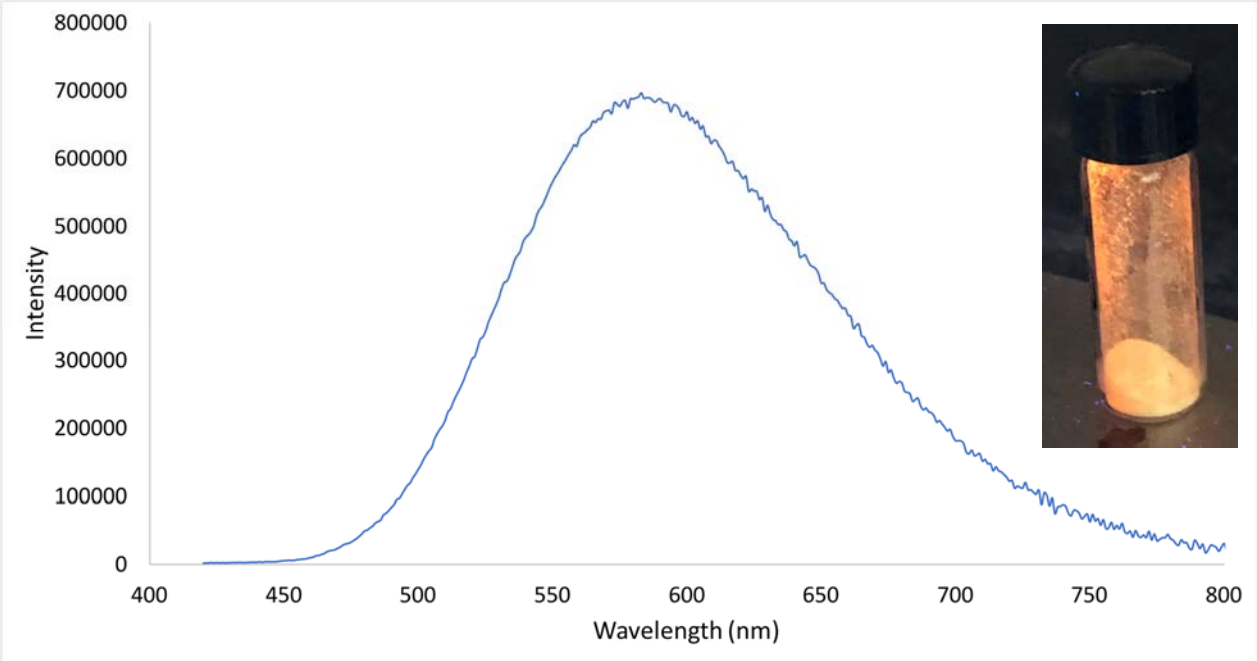

Figure S19. Emission spectrum taken of solid **2** excited at 365 nm. Inset: photograph of the solid-state emission of **2** after irradiation with a UV lamp.

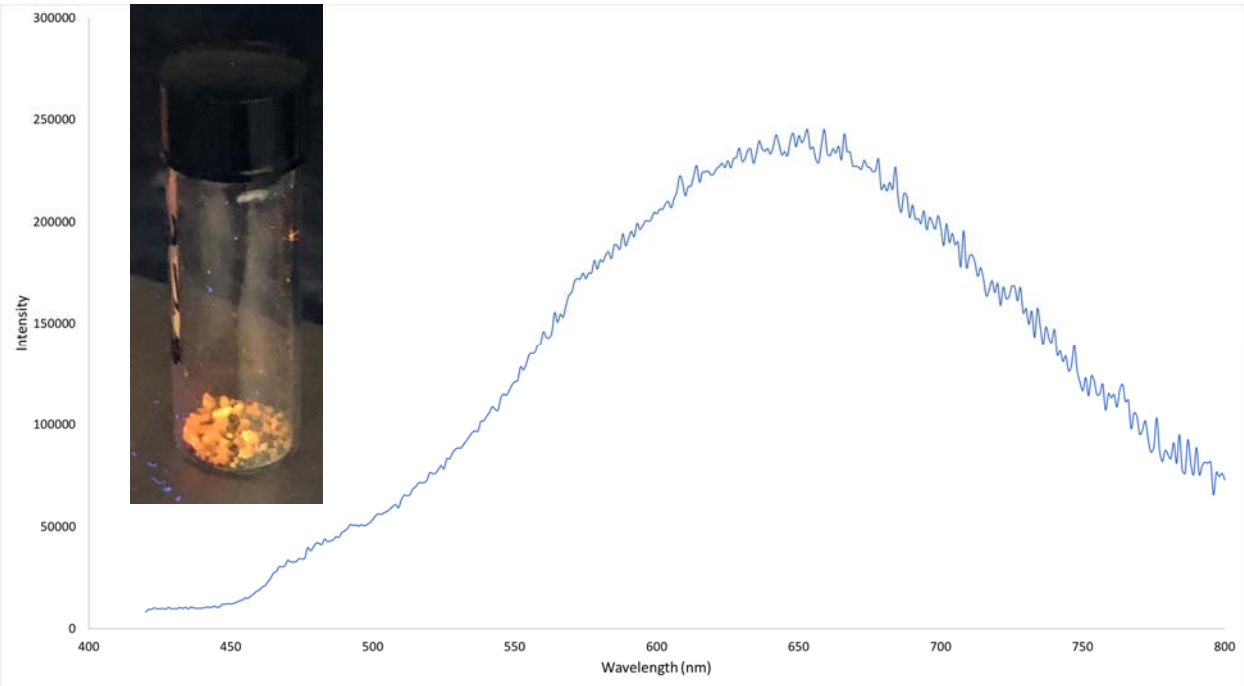

Figure S20. Emission spectrum taken of solid **3** excited at 365 nm. Inset: photograph of the solid-state emission of **3** after irradiation with a UV lamp.

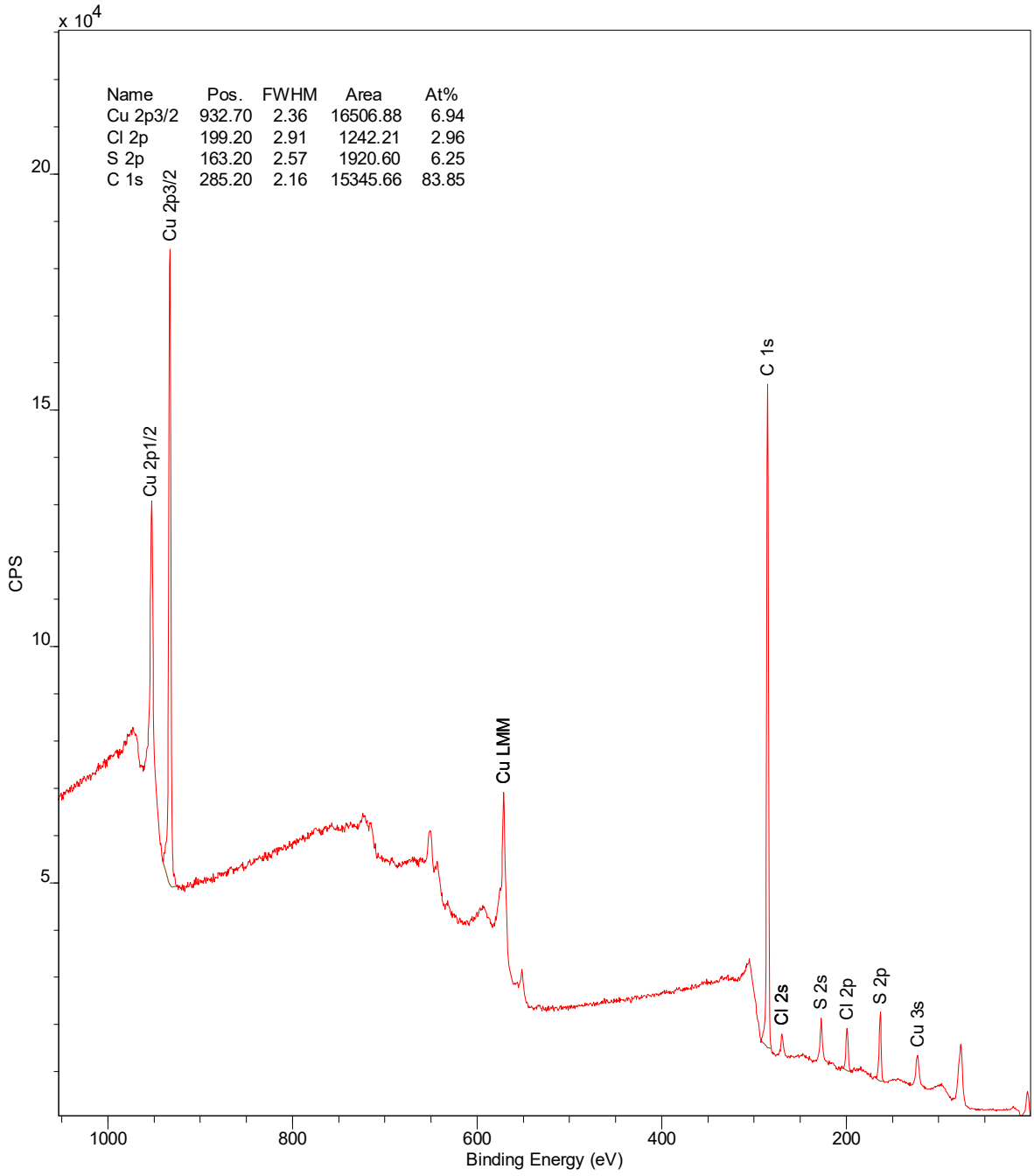

Figure S21. XPS spectrum of **1**, synthesized from THF, indicating a Cu:S:Cl ratio of approximately 2:2:1.

Table S2. X-ray photoelectron spectroscopy data.

Assignment	E_b (eV)
Cu 2p1/2	952.70
Cu 2p3/2	932.70
Cu LMM	575.0
Cu LMM	571.1
Cu LMM	568.3
C 1s	285.20
Cl 2s	269.70
S 2s	227.10
Cl 2p	199.20
S 2p	163.20
Cu 3s	123.10

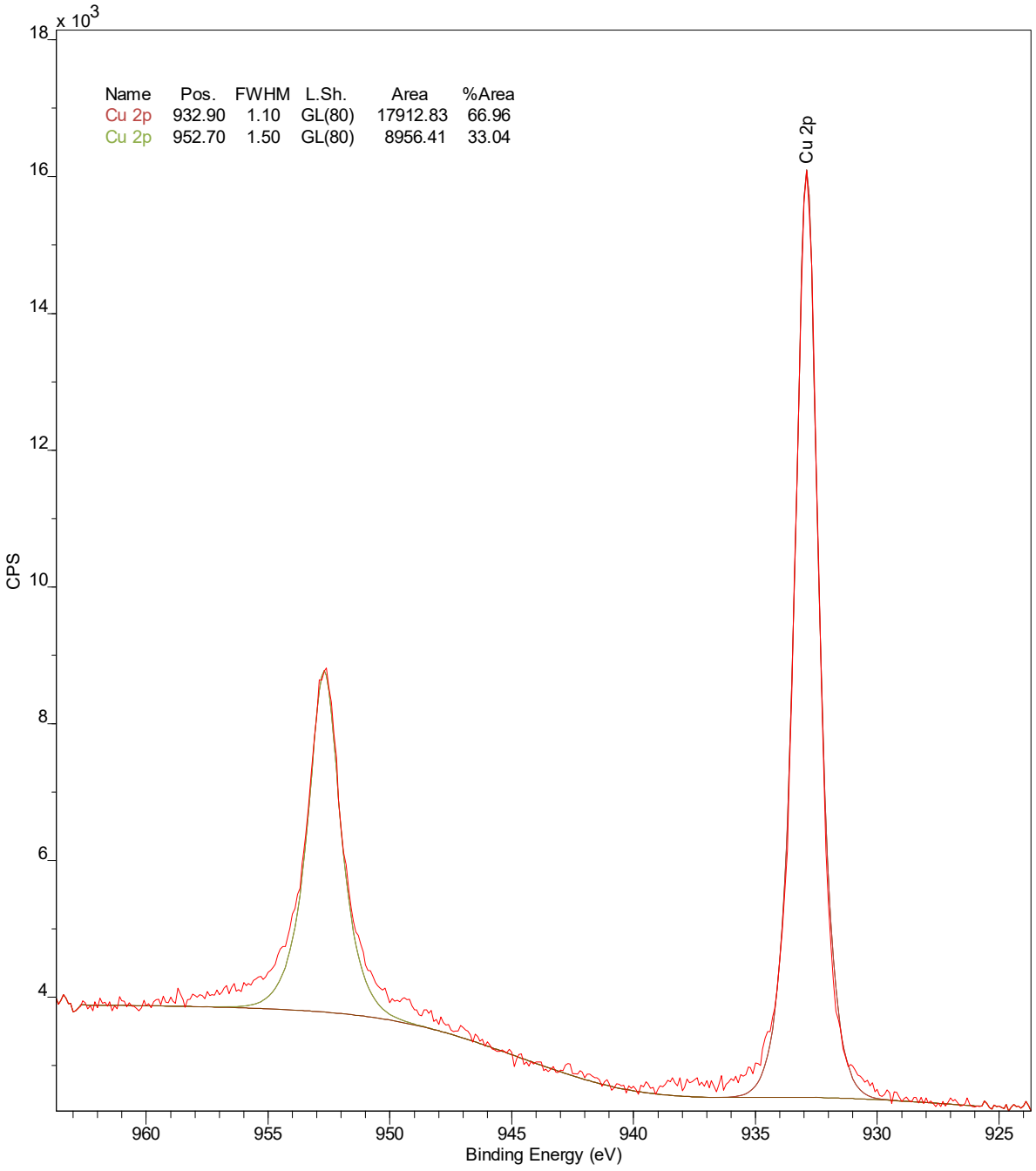

Figure S22. Partial XPS spectrum of **1**, synthesized from THF, showing the Cu(I) 2p transitions.

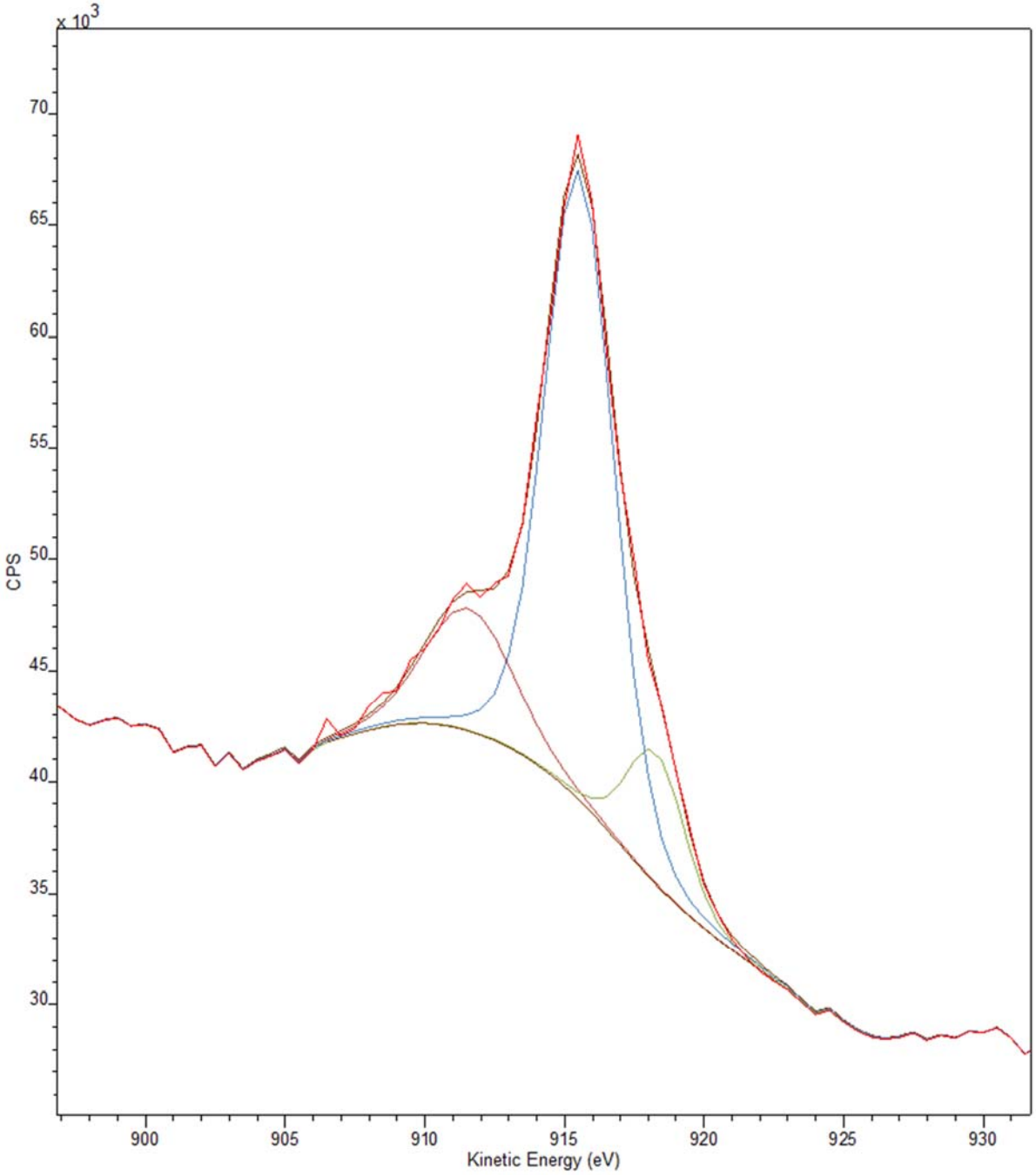

Figure S23. Partial XPS spectrum of **1**, synthesized from THF, showing the Cu(I) LMM transitions.

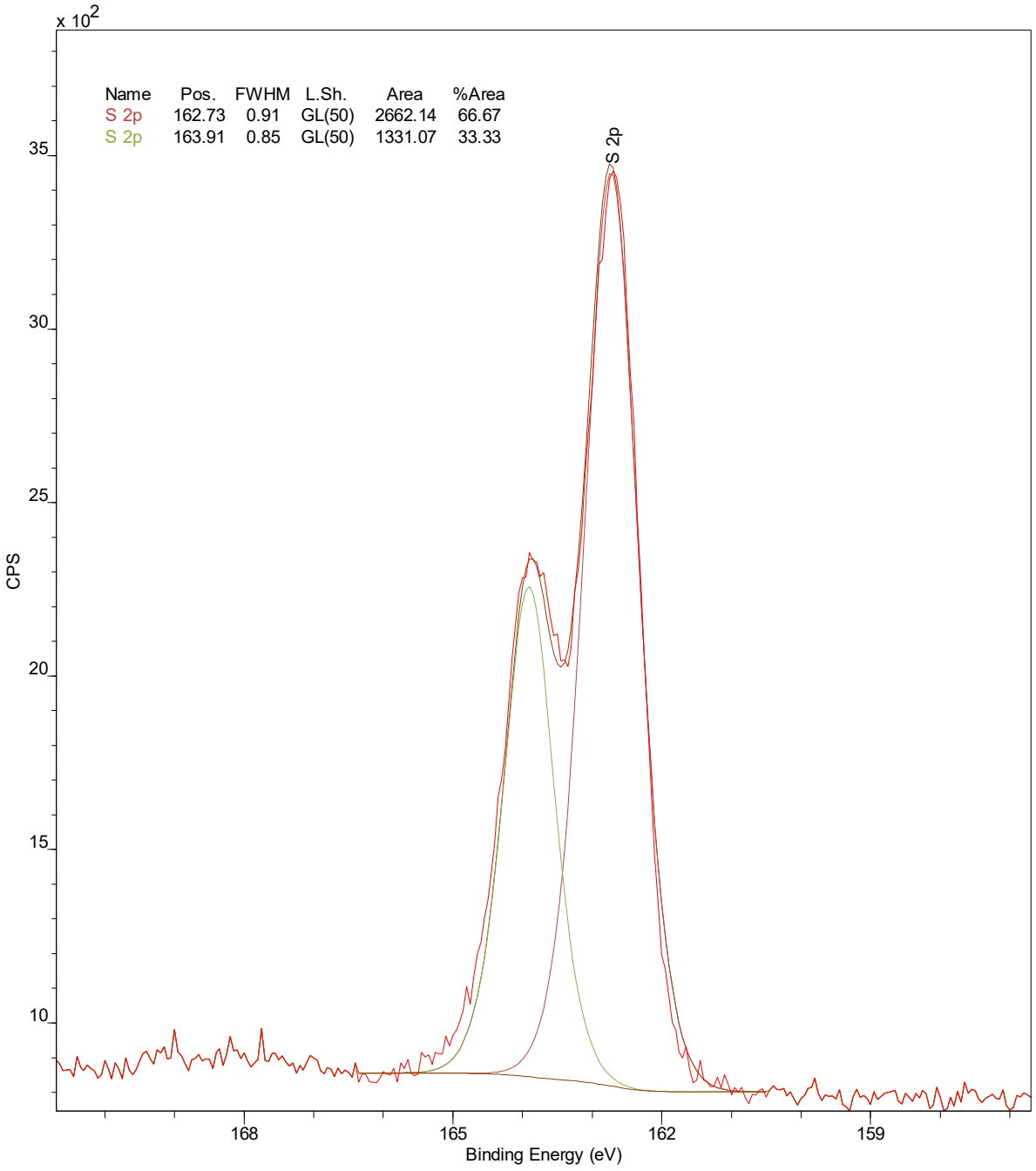

Figure S24. Partial XPS spectrum of **1**, synthesized from THF, showing the S 2p transitions.

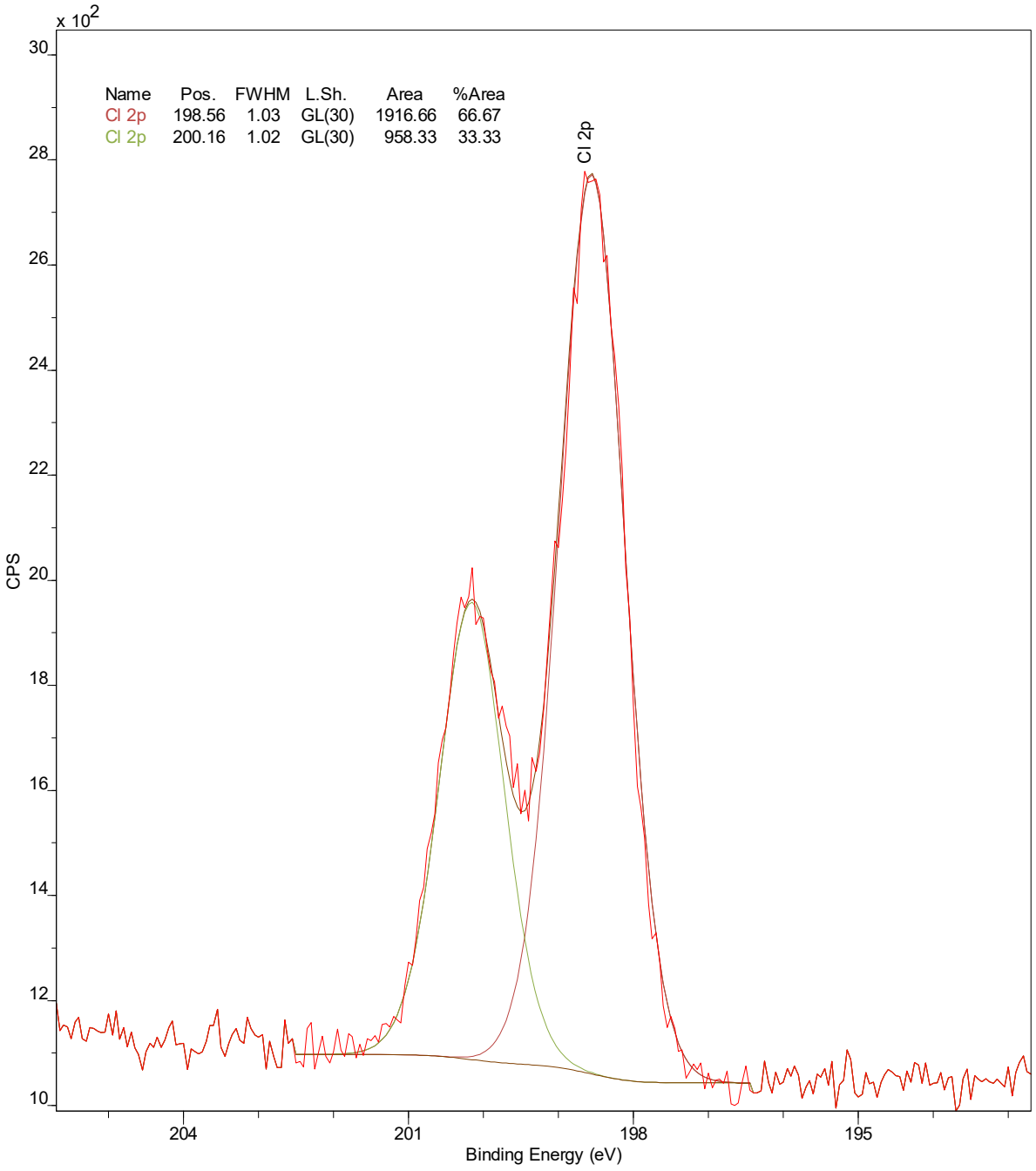

Figure S25. Partial XPS spectrum of **1**, synthesized from THF, showing the Cl 2p transitions.

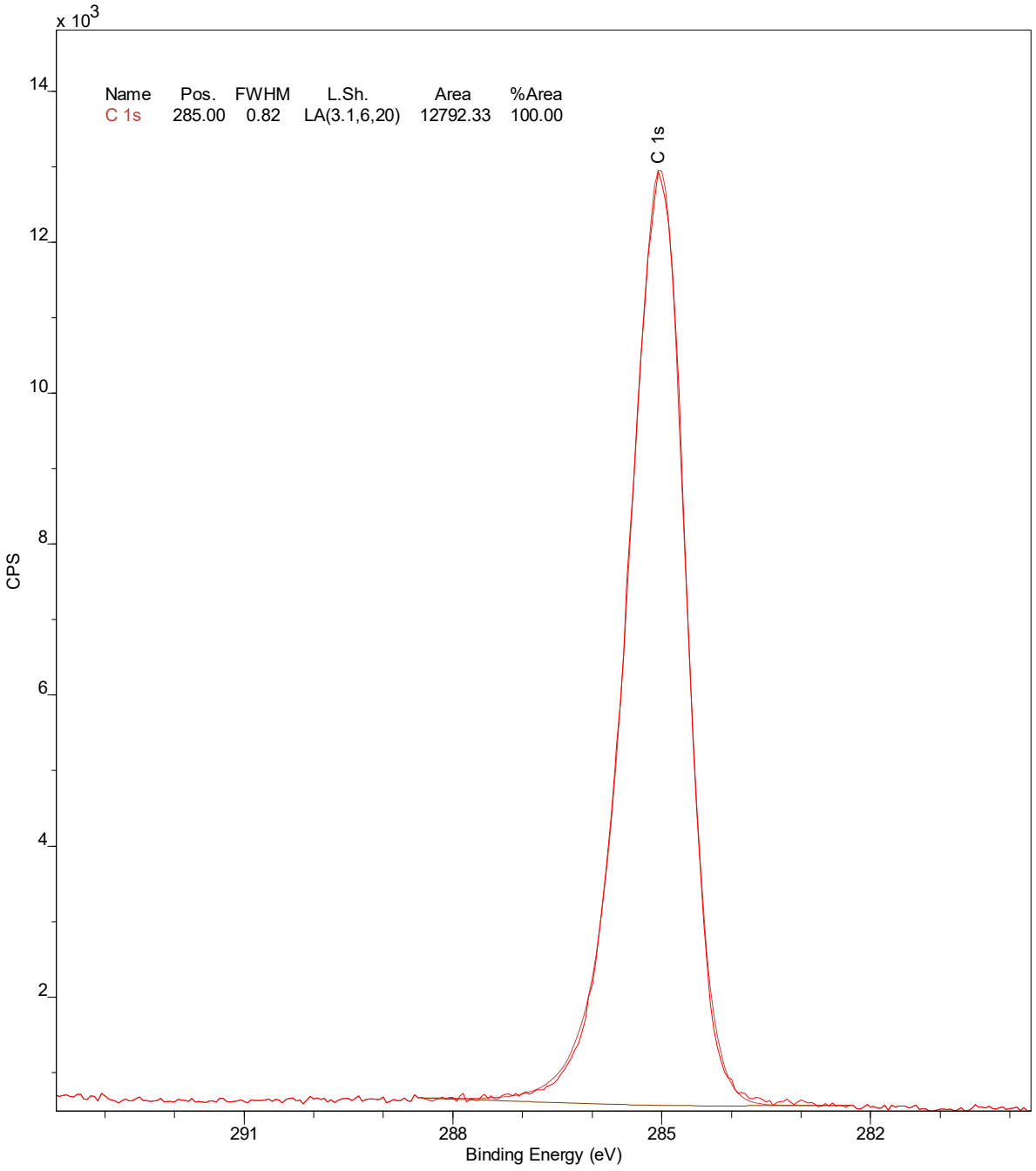

Figure S26. Partial XPS spectrum of **1**, synthesized from THF, showing the C 1s transition.

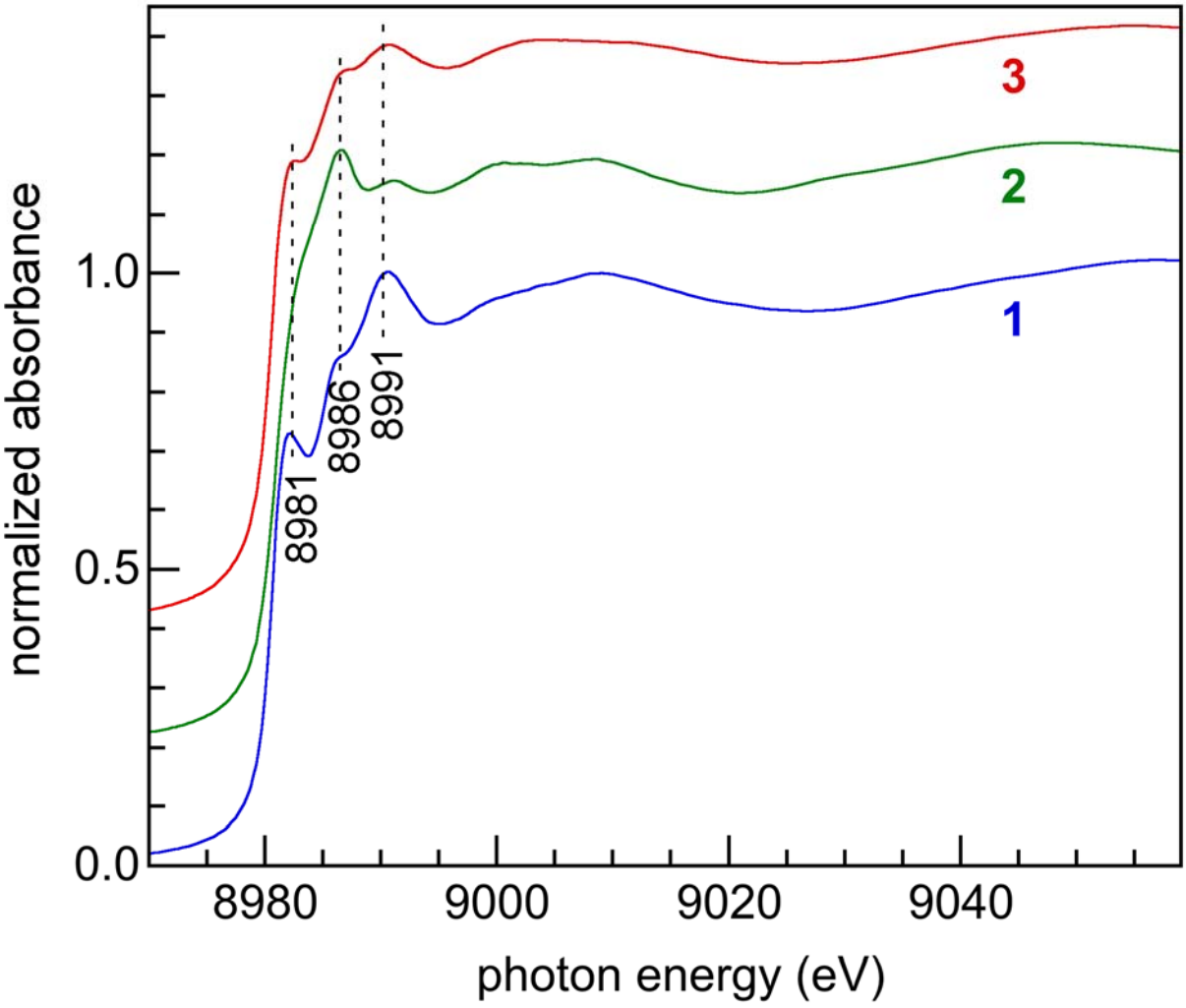

Figure S27. Comparison of Cu K-edge XANES of **1**, **2** and **3**. Spectra are offset vertically for clarity. For each cluster, the XANES profile includes three peaks, at 8981.0, 8986.0 and 8991.0 eV. These features arise from dipole-allowed $1s \rightarrow 4p$ transitions. Tetrahedrally-coordinated Cu ions are expected to show only $1s \rightarrow 4p$ excitations, while the trigonal planar Cu atoms will have distinct $1s \rightarrow 4p_{x,y}$ and $1s \rightarrow 4p_z$ transitions. The appearance of three peaks in the XANES is consistent with these assignments. However, their relative intensities vary for each cluster, likely due to variability in the number and type of non-core Cu atoms as a result of the different capping thiolate ligands (*n*-butanethiolate, ethylphenylthiolate, or *n*-dodecanethiolate).

EXAFS Analysis. Fits of the EXAFS data were initially performed with a single Cu-Cu path (Table S3). For all three nanoclusters, the refined Cu-Cu pathlengths exceed 2.7 Å. This distance is significantly longer than the expected value for metallic bonding (2.55 Å), but is consistent with the long interactions between Cu(I) ions. The results show generally good agreement with the "Atlas-sphere" model. However, the resulting values of *N*(Cu-Cu) are slightly lower than expected for nanoclusters **2** and **3**, while the corresponding σ^2 values are larger than expected (Table S3). Moreover, unlike $[Cu_{14}H_{12}(Ph_2phen)_6(PPh_3)_4][Cl]_2$, the "Atlas sphere" structure does not have near-collinear Cu-Cu-Cu paths to account for the intensity at ca. 4 Å. Triangular multiple-scattering paths involving Cu-S/Cl did not give good results. Instead, the long-range peak in the EXAFS of **1** was adequately modeled using only a Cu-Cu single-scattering path (represented as Cu-Cu2).

Table S3. Comparison of average FEFF-predicted paths for the 'Atlas-sphere' core $[Cu_{12}(SR)_6Cl_{12}]^{6-}$ with EXAFS curvefit parameters for nanoclusters **1**, **2**, and **3**, modeled using a single short Cu-Cu path.

Cluster	Path	N	R (Å)	$10^3\ \sigma^2$ (Å^2)	E_0 (eV)
$[Cu_{12}(SR)_6Cl_{12}]^{6-}$	Cu-L1	1.5	2.28(4)		
	Cu-Cu	2.0	2.76(14)		
	Cu-Cu2	2.9	4.03(15)		
1 [a]	Cu-L	1.9(3)	2.280(2)	3.9(3)	5.7(5)
	Cu-Cu1	2.0(3)	2.77(4)	7(1)	
	Cu-Cu2	2.4(4)	4.047(2)	8.9(5)	
2 [b]	Cu-L	1.2(2)	2.271(5)	3.0(9)	5.7(2)
	Cu-Cu	1.2(4)	2.76(4)	11(2)	
3 [c]	Cu-L	1.5(3)	2.298(6)	4.1(3)	4.7(5)
	Cu-Cu	1.1(2)	2.71(1)	12(4)	

[a] N_{idp} = 23, ΔR = 1.0 – 4.5 Å, Δk = 3.0 – 13.5 Å^{-1}. [b] N_{idp} = 15, ΔR = 1.0 – 3.0 Å, Δk = 3.0 – 14.5 Å^{-1}. [c] N_{idp} =13, ΔR = 1.0 – 3.0 Å, Δk = 3.0 – 13.3 Å^{-1}. In all fits, S_o^2 was fixed at 0.8, in accordance with our previous analyses of Cu(I) standards and Cu-based clusters,[3-4] and ΔE_0 was refined as a global fit parameter. Uncertainties are shown in parentheses; values without uncertainties were fixed during curvefitting.

EXAFS data for **1**, **2**, and **3** were also fitted with two difference Cu-Cu pathlengths. The results of the fits are shown in Table 1. For all three nanoclusters, refinement of two Cu-Cu paths results in Cu-Cu distances that differ by only ca. 0.2 Å, with the shorter path making a greater contribution to the spectrum due to its larger value of *N*. For **1**, the principal effect of two Cu-Cu paths (relative to only one Cu-Cu path; see above for details) is a reduction in the mean-squared displacements, while the combined value of *N*(Cu-Cu) remains unchanged at 2.0(5). For **2** and **3**, the average *N*(Cu-Cu) values increase significantly, to 1.9(4) and 2.3(5), respectively, while the σ^2 values remain unchanged (See Table 1). A second effect of including two Cu-Cu paths on N_{total}(Cu-Cu) is a dampening of the peak intensity, a consequence of destructive interference between the paths, which results in more accurate *N*(Cu-Cu) values. This is illustrated by the individual scattering paths for curvefits with two Cu-Cu paths (Figure S28).

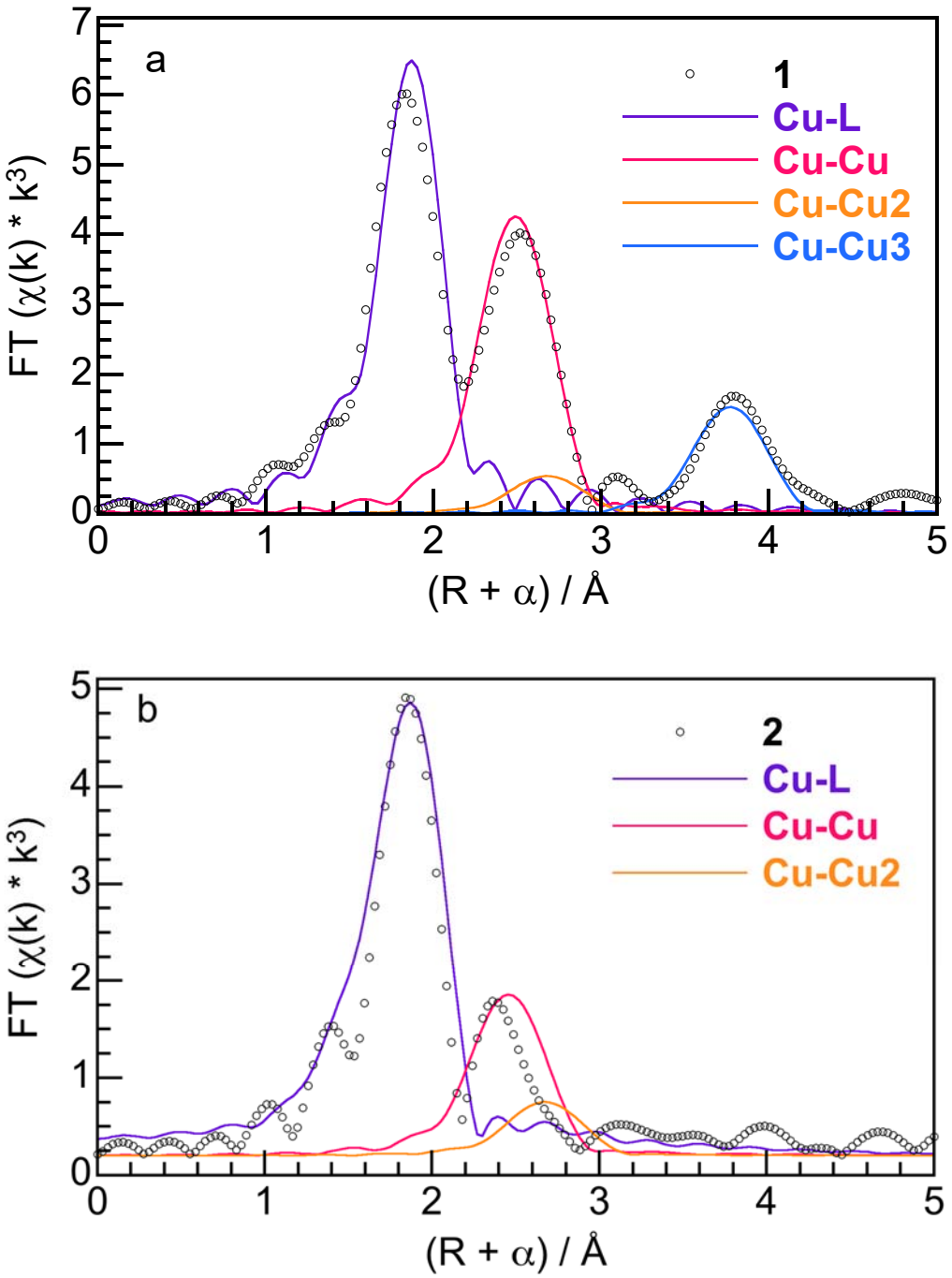

Figure S28. Individual scattering paths from the EXAFS curvefits of **1** and **2**, corresponding to the fits shown in Table 1.

Table S4. Curvefit parameters for the Cu K-edge EXAFS of $[Cu_{14}H_{12}(phen)_6(PPh_3)_4][Cl]_2$

Path	Crystal structure [a]		EXAFS		
	N	d (Å)	N	R (Å)	$10^3\ \sigma^2$ (Å^2)
Cu-N	0.86	2.104	0.86	2.067(10)	9(3)
Cu-P	0.3	2.294	0.3	2.300(10)	5(1)
Cu-Cu1	6[b]	2.51	1.7(2)	2.520(4)	6(1)[c]
Cu-Cu2		2.66	2.3(2)	2.658(4)	6(1)[c]
Cu-Cu3		2.90	0.1(1)	2.89(1)	6(1)[c]
Cu-Cu-Cu	6	4.31	2.7(5)	4.310	9(2)

[a] Average values, based on the published single-crystal X-ray diffraction structure.[2] [b] The Cu-Cu paths that occurred at distances with the highest frequency, predicted from the FEFF calculation, were modeled in the curvefit. N_{idp} =21, ΔR = 1.1 – 3.7 Å, Δk = 2.3 – 14.9 Å^{-1}. [c] The σ^2 values were constrained to the same parameter. The value of S_o^2 was fixed at 0.8, in accordance with our previous analyses of Cu(I) standards and Cu-based clusters,[3-4] ΔE_0 was refined as a global fit parameter, yielding ΔE_o = 6.0(4) eV. Uncertainties are shown in parentheses; values without uncertainties were fixed during curvefitting.

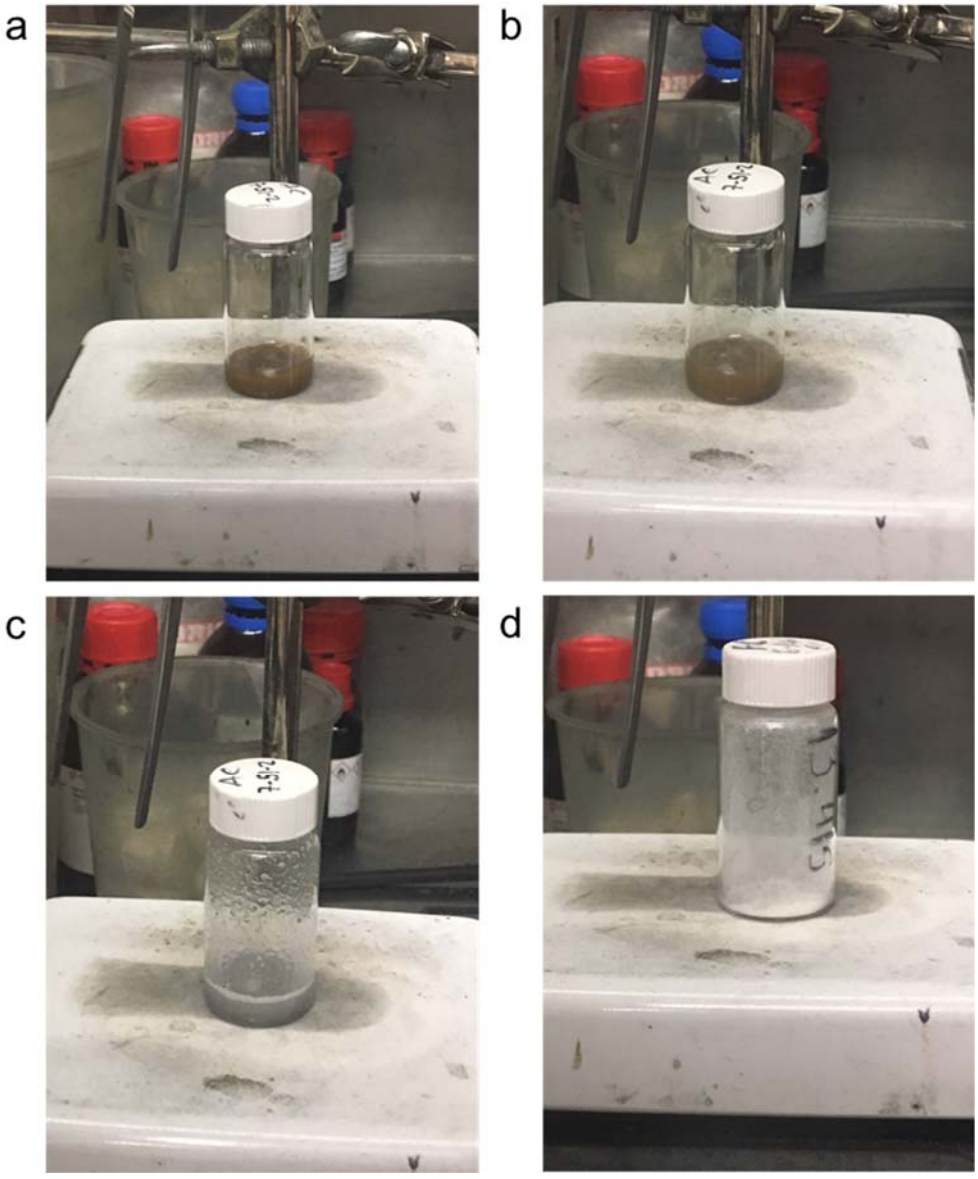

Figure S29. Photographs following the progress of the reaction between $CuCl_2$ and $HSC_{12}H_{25}$ (4 equiv) in dibenzyl ether (2 mL) at various reaction times. (a) $CuCl_2$ in dibenzyl ether, (b) 20 s after addition of thiol, (c) 20 min, (d) isolated powder of **1**.

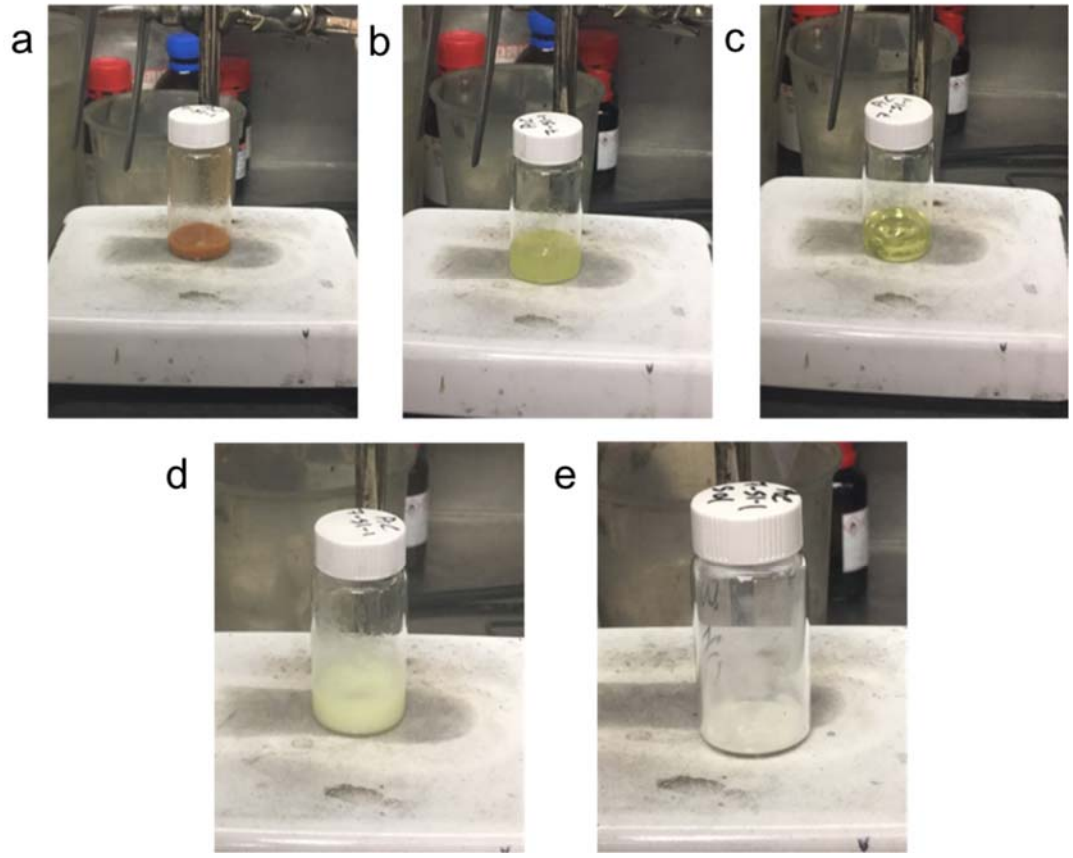

Figure S30. Photographs following the progress of the reaction between $CuCl_2$ and $HSC_{12}H_{25}$ (4 equiv) in THF (2 mL) at various reaction times. (a) $CuCl_2$ in THF, (b) 20 s after addition of thiol, (c) 5 min, (d) 20 min, (e) isolated powder of **1**.

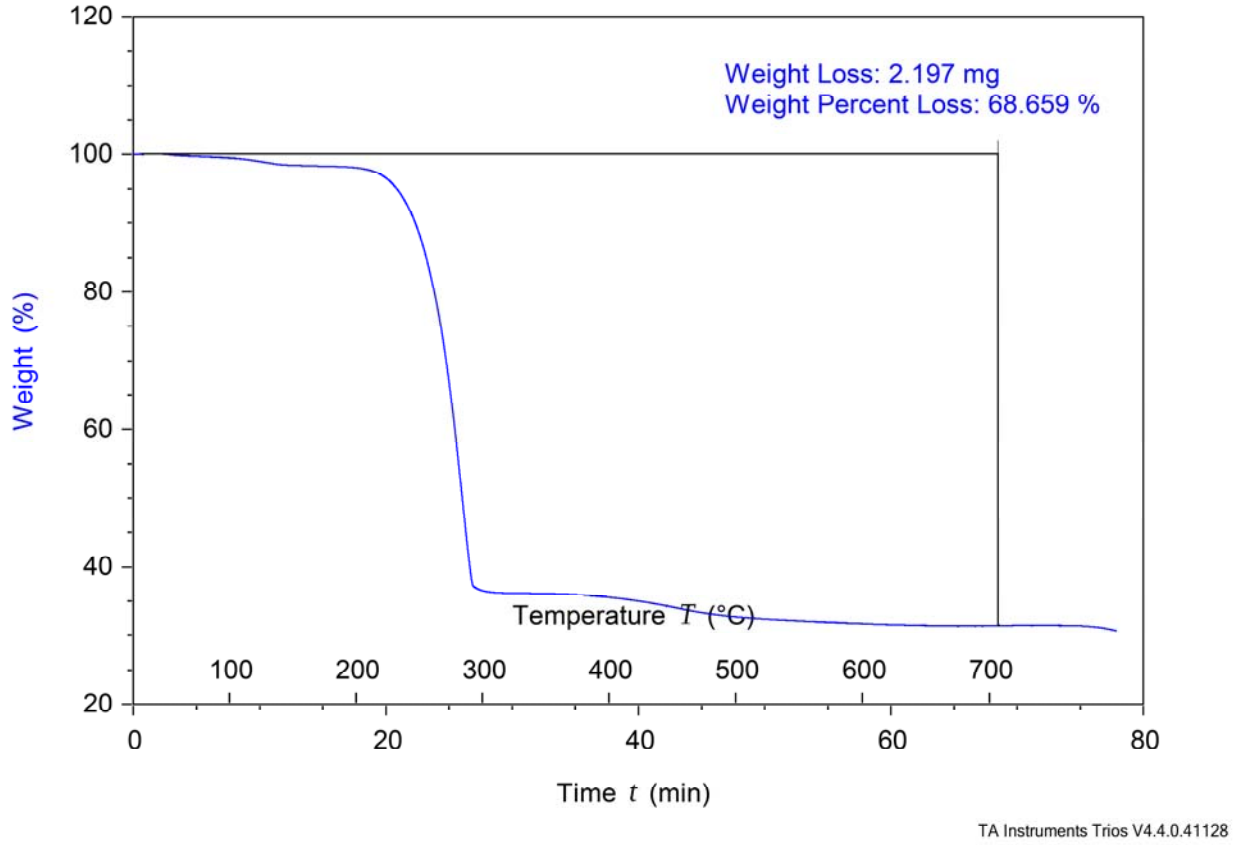

Figure S31. TGA profile of complex **1**. Ramp rate: 10 °C/min; N_2 flow rate: 25 mL/min.

References:

1. Cook, A. W.; Wu, G.; Hayton, T. W., A Re-examination of the Synthesis of Monolayer-Protected $Co_x(SCH_2CH_2Ph)_m$ Nanoclusters: Unexpected Formation of a Thiolate-Protected Co(II) T3 Supertetrahedron. *Inorg. Chem.* **2018**, *57*, 8189-8194.
2. Nguyen, T.-A. D.; Goldsmith, B. R.; Zaman, H. T.; Wu, G.; Peters, B.; Hayton, T. W., Synthesis and Characterization of a Cu_{14} Hydride Cluster Supported by Neutral Donor Ligands. *Chem. – Eur. J.* **2015**, *21*, 5341-5344.
3. Nguyen, T.-A. D.; Jones, Z. R.; Leto, D. F.; Wu, G.; Scott, S. L.; Hayton, T. W., Ligand-Exchange-Induced Growth of an Atomically Precise Cu_{29} Nanocluster from a Smaller Cluster. *Chem. Mater.* **2016**, *28*, 8385-8390.
4. Cook, A. W.; Jones, Z. R.; Wu, G.; Scott, S. L.; Hayton, T. W., An Organometallic Cu_{20} Nanocluster: Synthesis, Characterization, Immobilization on Silica, and "Click" Chemistry. *J. Am. Chem. Soc.* **2018**, *140*, 394-400.
5. Ravel, B.; Newville, M., ATHENA, ARTEMIS, HEPHAESTUS: data analysis for X-ray absorption spectroscopy using IFEFFIT. *J. Synchrotron Rad.* **2005**, *12*, 537-541.
6. Wu, Z.; Liu, J.; Gao, Y.; Liu, H.; Li, T.; Zou, H.; Wang, Z.; Zhang, K.; Wang, Y.; Zhang, H.; Yang, B., Assembly-Induced Enhancement of Cu Nanoclusters Luminescence with Mechanochromic Property. *J. Am. Chem. Soc.* **2015**, *137*, 12906-12913.
7. Higuchi, O.; Tateshita, K.; Nishimura, H., Antioxidative Activity of Sulfur-Containing Compounds in Allium Species for Human Low-Density Lipoprotein (LDL) Oxidation in Vitro. *J. Agric. Food Chem.* **2003**, *51*, 7208-7214.
8. Scholz, S.; Lerner, H.-W.; Bolte, M., Chlorotripyridinecopper(I). *Acta Cryst. E.* **2002**, *58*, m72-m73.
9. *SMART Apex II, Version 2.1*. Bruker AXS Inc.: Madison, WI, 2005.
10. *SAINT Software User's Guide, Version 7.34a*. Bruker AXS Inc.: Madison, WI, 2005.
11. Sheldrick, G. M., *SADABS*. University of Göttingen: Göttingen, Germany, 2005.
12. *SHELXTL PC, Version 6.12*. Bruker AXS Inc.: Madison, WI, 2005.
13. Hasan, M.; Bethell, D.; Brust, M., The Fate of Sulfur-Bound Hydrogen on Formation of Self-Assembled Thiol Monolayers on Gold: ^{1}H NMR Spectroscopic Evidence from Solutions of Gold Clusters. *J. Am. Chem. Soc.* **2002**, *124*, 1132-1133.